

## 3-loop 3PI effective action for 3D SU(3) QCD

---

**Mark C. Abraao York, Guy D. Moore, Marcus Tassler**

*McGill University Department of Physics  
3600 Rue University  
Montreal, QC  
H3A 2T8*

ABSTRACT: The 3PI method is a technique to resum an infinite class of diagrams, which may be useful in studying nonperturbative thermodynamics and dynamics in quantum field theory. But it has never been successfully applied to gauge theories, where there are serious questions about gauge invariance breaking. We show how to perform the 3PI resummation of QCD in 3 Euclidean spacetime dimensions, a warmup problem to the 4 or 3+1 dimensional case. We present the complete details of the technical problems and how they are overcome. We postpone a comparison of gauge invariant correlation functions with their lattice-determined counterparts to a future publication.

ARXIV EPRINT: [1202.4756](https://arxiv.org/abs/1202.4756)

---

## Contents

<b>1</b>	<b>Introduction</b>	<b>1</b>
<b>2</b>	<b>The 3PI Effective Action</b>	<b>5</b>
<b>3</b>	<b>Divergences and Regularization</b>	<b>8</b>
3.1	Divergences in self-energies	8
3.2	Divergences upon $p$ -integration	14
<b>4</b>	<b>Variational <i>Ansätze</i></b>	<b>15</b>
4.1	Numerical Implementation	19
<b>5</b>	<b>Results</b>	<b>25</b>
<b>6</b>	<b>Discussion</b>	<b>27</b>
6.1	Comparison with other approaches	27
6.1.1	The Gribov-Zwanziger Confinement Hypothesis	29
6.1.2	Schwinger-Dyson Equations	29
6.1.3	Observations From the Lattice	29
6.2	Slavnov-Taylor Identities	30
<b>7</b>	<b>Conclusions</b>	<b>32</b>
<b>A</b>	<b>Computations involving Bare Diagrams</b>	<b>33</b>
A.1	Gluon Self-Energy	33
A.2	Ghost Self-Energy	36
A.3	Three-Gluon and Ghost-Gluon Vertices	36
<b>B</b>	<b>Phase space integrations</b>	<b>40</b>
B.1	Two loops: Setting Sun	40
B.2	Three loops: Mercedes	41

---

## 1 Introduction

The early Universe existed in a state of deconfined quark-gluon plasma, a state which has also recently been produced in the laboratory via heavy ion collisions. The thermodynamics of such plasmas are now relatively well understood. In the early Universe the gross features are well described by perturbation theory, and while the strength of the electroweak phase transition (or crossover) cannot in general be determined perturbatively, there are powerful lattice methods which can be brought to bear [1]. Lattice methods can also describe the

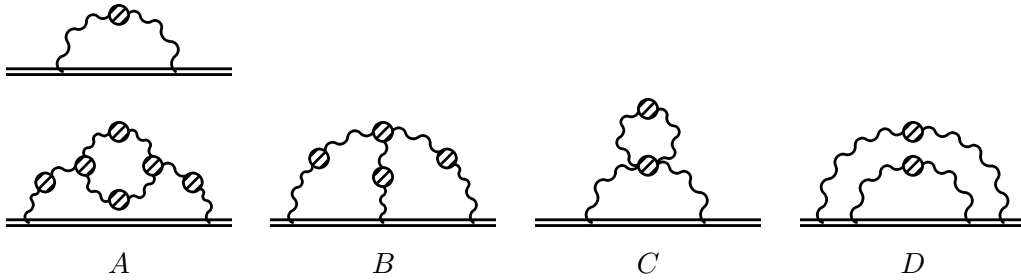


**Figure 1.** NLO heavy quark diffusion.

thermodynamics of QCD near its intrinsic scale  $\Lambda_{\text{QCD}}$ , provided that the chemical potential is not too large [2–4]. However, many of the most interesting questions in each context have to do with dynamics or unequal time correlations. For instance, real-time correlations and nonequilibrium currents are important in understanding whether electroweak baryogenesis can occur at a first order electroweak phase transition [5, 6]. In the heavy ion context there are many dynamical quantities we would like to know, such as the viscosity [7–10], heavy quark diffusion rate [11–13], photon production rate [14–16], and so forth. Dynamical properties of QCD are also important at much higher temperatures such as the electroweak temperature, where they could play a role in baryogenesis and in various phase transitions.

The problem is that we have no first-principles, intrinsically nonperturbative technique for theoretically predicting such real-time properties, even in equilibrium or linear response. We have models and phenomenological fitting (for instance, of the viscosity using elliptic flow in heavy ion collisions [10]), but the only tool we have which is close to first principles is perturbation theory.

Perturbation theory is notoriously poorly convergent when applied to hot gauge theories. For instance, the expansion for the pressure of QCD as a series in  $\alpha_s$  is known to order  $\alpha_s^3 \ln \alpha_s$ , but the series only appears to be useful at temperatures many times the scale  $\Lambda_{\text{QCD}}$  [17]. For real-time quantities, certain (Hard Thermal Loop or HTL) resummations [18] are necessary even to find leading order results for transport coefficients [19, 20]. Even so, the perturbative expansion for real-time quantities appears to be even worse behaved than it is for the pressure and other thermodynamic quantities, at least if we restrict attention to transport coefficients, which involve either zero frequency and momentum or lightlike momentum limits of external 4-momenta. Only two such quantities are known beyond leading order; the diffusion coefficient for a heavy quark [21] and the transverse momentum diffusion for a fast charge [22]. In each case the first corrections enter at order  $g$ , not order  $g^2$  as would be normal in a vacuum perturbative expansion, and the corrections represent of order 100% shifts in the transport coefficients for  $\alpha_s \sim 0.05$ , a value obtained only at temperatures well above 1 TeV! Though it is a little dangerous to extrapolate from two examples, it appears that even at the electroweak scale, the QCD sector of the Standard Model is probably not well described by perturbation theory, as far as dynamics are concerned.

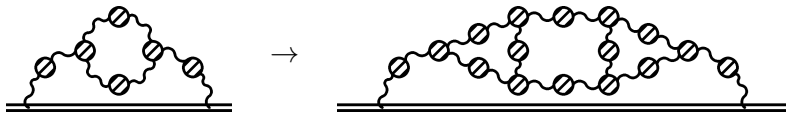


**Figure 2.** Inclusion of additional HTLs.

Let us analyze the problem in a little more detail, for the case of heavy quark diffusion [21]. The leading-order diagram and the four next-to-leading order diagrams are shown in Fig. 1. Here the double line is the Wilson line heavy quark trajectory, and hatched blobs represent Hard Thermal Loop (HTL) resummation. In particular, the leading-order diagram is already one-loop self-energy resummed. The contribution from diagram *A* is 5 to 10 times as large as that of the other diagrams (in Coulomb gauge, the choice used in [21]). Therefore the physics which is problematic for the perturbative expansion is presumably the physics represented by this diagram. This diagram resembles the leading-order diagram, except that in the leading diagram the momentum in the self-energy loop is assumed to be large compared to the propagator momentum, while in diagram *A* it is allowed to be of the same order. When the momentum is soft, it is also necessary to include HTLs on the propagators and vertices of the self-energy in diagram *A*. The large size of diagram *A* indicates that the soft loop momentum region in the self-energy is almost as important as the region where the loop momentum is hard. This is a problem because in this soft region, the HTL corrections must also be included on the propagators and vertices in diagram *A*. But why shouldn't these loops also receive large corrections from their soft-momentum regions? Then we also need to include the region where we replace the HTLs in diagram *A* with soft momenta, as suggested in Fig. 2. But when these momenta are soft, there are new vertices and propagators requiring HTL corrections. These may also have large soft corrections, bringing in more diagrams – and we are “off to the races.”

The problem is that the low-momentum ( $gT$ ) region is not really a small part of phase space, and it is not really weakly coupled. But the good news is that the dominance of diagram *A* above suggests that it is really only the soft corrections to the HTLs present in the previous order which are important. This leads to an infinite number of diagrams contributing, but only a restricted (infinite) set of diagrams being “most important” – those suggested at in Fig. 2. If these diagrams could be resummed somehow, then we would likely capture all the most important corrections, and the range of validity of perturbation theory might be significantly expanded.

There *is* a procedure for performing an iterative resummation of all one-loop self-energy and 3-point vertex corrections, as suggested in Fig. 2. It is the 3-loop, 3-particle irreducible (3PI) resummation scheme [23, 24]. The above discussion suggests that a 3PI resummation may capture the most important higher-order physics and greatly improve the convergence of the perturbative expansion – even capturing some nonperturbative information. But this is by no means guaranteed, since the 3PI approach performs an incomplete resummation of higher-order effects, which furthermore is not gauge invariant. We would like, eventually, to perform a 3-loop 3PI resummation of real-time, 3+1 dimensional QCD (or the full

Standard Model) at small or intermediate coupling. However, as yet the 3PI technique has never been applied to nonabelian gauge theories. And we would also like to *test* whether the resummation technique is effective and reliable in a somewhat more controlled setting. Therefore we feel it is necessary to consider a slightly simpler problem as a warm-up exercise, and as a testing ground for whether the 3PI technique is effective in nonabelian gauge theory. Therefore, in this work we will investigate the 3-loop, 3PI resummation of *3-dimensional* (3D), SU(3) Yang-Mills theory, an endeavor we will call the “all threes” problem (3D, 3-loop 3PI for SU(3)).

Working in 3 Euclidean dimensions simplifies our problem in two ways. First, the UV behavior of 3D Yang-Mills theory is much milder than in 4D, since the theory is super-renormalizable. The second simplification is that the vacuum Euclidean theory has fewer Lorentz invariants than the finite-temperature, Minkowski theory (or the Euclidean theory with periodic time direction). For instance, in (vacuum) Euclidean space the propagator  $G^{\mu\nu}$  is built from two tensorial structures and is a function of one invariant;  $G^{\mu\nu}(p) = \mathbf{T}^{\mu\nu}G_T(p^2) + \mathbf{L}^{\mu\nu}G_L(p^2)$ . In real time at finite temperature, or in imaginary time with periodic boundary conditions, it has more tensorial structures and is a function of *two* variables,  $p^2$  and the energy  $p^0$ .

Note however that 3D Yang-Mills theory is far from trivial. The flip side of super-renormalizability is that, since the gauge coupling is dimensionful, it establishes a scale (momentum scale  $p \sim g^2$  or length scale  $\lambda \sim 1/g^2$ ) where we expect strongly coupled, nonperturbative behavior. Therefore 3D Yang-Mills theory displays both weak or strong coupling, depending on the energy scale. 3D Yang-Mills theory is also physically interesting. At the thermodynamic level, the infrared behavior of thermal 4D Yang-Mills theory (with any fermionic matter content) is 3D Yang-Mills with an adjoint scalar [25–27], a slight extension of the problem we consider. The nonperturbative scale  $g^2 \equiv g_{3D}^2$  corresponds to the scale  $g_{4D}^2 T$  of the full theory (at leading perturbative order). It is believed that the poor convergence of perturbation theory at intermediate couplings in QCD is due to the nonperturbative physics of the 3D theory. Therefore in a sense studying the 3D gauge theory by nonperturbative means is treating most of the physics which makes thermal QCD poorly behaved (at intermediate couplings).

The goal of this paper is to produce a complete solution to the 3-loop truncation of the 3PI effective action for 3D QCD. As outlined above, this should be viewed as a warm-up problem to what we would really like to do, which is to apply the resummation in 3+1 dimensions in a thermal (or even nonequilibrium) context. We feel that this first step is well motivated. As already emphasized, the 3D theory is a subset of the 3+1D theory (the theory we really want to solve). And the 3D theory can be studied nonperturbatively on a lattice, which means we will be able to test the 3PI resummation procedure in a nonperturbative context by seeing whether its predictions are successful. Such a test is necessary because the 3PI resummation captures only an incomplete and gauge-noninvariant subset of diagrams, so there is no hard guarantee that it will successfully reproduce the nonperturbative IR physics. This paper will concentrate on the resummation; we will return to the comparison with nonperturbative lattice studies in a follow-up publication.

## 2 The 3PI Effective Action

The 3PI effective action is obtained by a Legendre transform of the generating functional of connected diagrams

$$W[J, K, L] = -\log \int \mathcal{D}\phi e^{-\left(S[\phi] + J\phi + \frac{1}{2}K\phi^2 + \frac{1}{6}L\phi^3\right)} \quad (2.1)$$

with one, two and three-particle sources,  $J$ ,  $K$  and  $L$  (our notation is schematic, with fields generically denoted by  $\phi$  and matrix indices and space integrations suppressed). Conjugate to  $J$ ,  $K$  and  $L$  are the variables  $\bar{\phi}$ ,  $G$  and  $G_3$ , which are labelled as such since it can be proven that they are equal to the connected one, two and three-point functions. The functional derivatives of  $W$  are given by

$$\frac{\delta W}{\delta J} = \bar{\phi} \quad (2.2)$$

$$\frac{\delta W}{\delta K} = \frac{1}{2}(G + \bar{\phi}^2) \quad (2.3)$$

$$\frac{\delta W}{\delta L} = \frac{1}{6}(G_3 + 3G\bar{\phi} + \bar{\phi}^3), \quad (2.4)$$

and the 3PI effective action follows,

$$\Gamma[\bar{\phi}, G, G_3] = J \frac{\delta W}{\delta J} + K \frac{\delta W}{\delta K} + L \frac{\delta W}{\delta L} - W[J, K, L].$$

From Eqs. (2.3) and (2.4), we see that  $W$  generates connected as well as disconnected diagrams<sup>1</sup>, so it does not, strictly speaking, generate cumulants. However,  $W$  is still equal to the logarithm of a moment generating functional, hence one can expect that it as well as its Legendre transform  $\Gamma$  have well defined extrema. In terms of  $\Gamma$  the equations of motion for  $\bar{\phi}$ ,  $G$  and  $G_3$  read

$$\frac{\delta \Gamma}{\delta \bar{\phi}} = \frac{\delta \Gamma}{\delta G} = \frac{\delta \Gamma}{\delta G_3} = 0. \quad (2.5)$$

We will now specialize this procedure to the case of QCD. Since we consider pure-gluon QCD there is no Higgs mechanism and we expect the one-point functions to vanish at the extremum<sup>2</sup>; hence we can set the VEVs of  $A^\mu$ ,  $\bar{c}$  and  $c$  to zero and work only with the two and three-point functions. To write down the exact form of  $\Gamma$  relevant to the QCD<sub>3</sub> field content, it is useful to define the propagators and vertex functions<sup>3</sup> listed in Table 1. The one-particle-irreducible 3-vertex  $V$  is related to the three-point function via  $G_3 = G^3 V$ ; extremizing with respect to  $G$  and  $G_3$  is equivalent to extremizing with respect to  $G$  and  $V$ , which we find to be more convenient variables. The 3PI effective action is given in terms of  $G$ ,  $\Delta$ ,  $V$  and  $\mathbb{V}$  by

<sup>1</sup>For instance,  $\delta\Gamma/\delta K$  generates  $\bar{\phi}^2 \equiv \langle \phi \rangle^2$ .

<sup>2</sup>When Grassman fields such as ghosts are present, the extremum is generally a saddle-point rather than a maximum.

<sup>3</sup>Throughout this work, we will generally suppress color indices and will frequently also suppress Lorentz indices, when the indices can be inferred from context. For instance,  $G = G_{\mu\nu} = G_{\mu\nu}^{ab}$ ,  $V_{\mu\nu\rho} = V_{\mu\nu\rho}^{abc}$  etc.

	Resummed	Bare
Gluon Propagator	$G_{\mu\nu}^{ab} = \text{wavy line}$	$G_{\mu\nu}^{(0)ab} = \text{wavy line}$
Ghost Propagator	$\Delta^{ab} = \text{dashed line with arrow}$	$\Delta^{(0)ab} = \text{dashed line with arrow}$
Gluon 3-Vertex	$V_{\mu\nu\rho}^{abc} = \text{three wavy lines meeting at a vertex}$	$gV_{\mu\nu\rho}^{(0)abc} = \text{three wavy lines meeting at a vertex}$
Ghost-Gluon Vertex	$\mathbb{V}_{\mu}^{abc} = \text{dashed line with arrow and wavy line meeting at a vertex}$	$g\mathbb{V}_{\mu}^{(0)abc} = \text{dashed line with arrow and wavy line meeting at a vertex}$
Gluon 4-Vertex	$V_{\mu\nu\rho\tau}^{abcd} = \text{four wavy lines meeting at a vertex}$	$g^2V_{\mu\nu\rho\tau}^{(0)abcd} = \text{four wavy lines meeting at a vertex}$

Table 1. Feynman Rules for QCD<sub>3</sub>

$$\begin{aligned}
\Gamma = & S[A^\mu, \bar{c}, c] + \frac{1}{2} \text{Tr} \log G - \frac{1}{2} \text{Tr}[G^{(0)}]^{-1} G - \text{Tr} \log \Delta + \text{Tr}[\Delta^{(0)}]^{-1} \Delta \\
& + \frac{1}{6} \text{diagram} - \frac{1}{12} \text{diagram} + \frac{1}{8} \text{diagram} \\
& - \text{diagram} + \frac{1}{2} \text{diagram} \\
& + \frac{1}{48} \text{diagram} + \frac{1}{24} \text{diagram} + \frac{1}{8} \text{diagram} \\
& - \frac{1}{3} \text{diagram} - \frac{1}{4} \text{diagram}, \tag{2.6}
\end{aligned}$$

(where we have explicitly written symmetry factors associated with diagrams and signs associated with ghost loops for clarity, as we will throughout), from which we have the following four equations of motion

$$\frac{\delta\Gamma}{\delta G} = \frac{\delta\Gamma}{\delta\Delta} = \frac{\delta\Gamma}{\delta V} = \frac{\delta\Gamma}{\delta\mathbb{V}} = 0. \tag{2.7}$$

To illustrate the physics of Eq. (2.7), consider  $\delta\Gamma/\delta G(p)$ . Performing the variation

using the expression in Eq. (2.6), we find

$$G^{-1}(p) = [G^0]^{-1}(p) - \Pi(p), \quad (2.8)$$

$$\Pi^{(1)}(p) = \text{[diagram 1]} - \frac{1}{2} \text{[diagram 2]} + \frac{1}{2} \text{[diagram 3]} - 2 \text{[diagram 4]} + \text{[diagram 5]}$$

which we recognize as the resummed one-loop self-energy ( $\Pi = \Pi^{(1)} + \Pi^{(2)}$ , we have not shown the similar graphical representation of  $\Pi^{(2)}$ ). Similarly, variation with respect to  $V$  gives

$$\text{[diagram 1]} = \text{[diagram 2]} + \text{[diagram 3]} + \frac{3}{2} \text{[diagram 4]} - 2 \text{[diagram 5]} \quad (2.9)$$

which we recognize as a Schwinger-Dyson equation for vertex resummation.

Note that the propagators appearing in all diagrams in Eq. (2.8) and Eq. (2.9), as well as all vertices (except certain vertices in the one-loop self-energies), are the full objects. Therefore these equations must be solved *self-consistently*. The self-consistent solution of these equations represents our main challenge. We face two chief difficulties:

- Decomposing the propagator into its transverse and longitudinal parts,

$$G^{\mu\nu}(p) = G_T^{\mu\nu}(p)\mathbf{T}^{\mu\nu} + G_L^{\mu\nu}(p)\mathbf{L}^{\mu\nu},$$

$$\mathbf{L}^{\mu\nu} \equiv \frac{p^\mu p^\nu}{p^2}, \quad \mathbf{T}^{\mu\nu} \equiv g^{\mu\nu} - \mathbf{L}^{\mu\nu}, \quad (2.10)$$

the propagators are determined in terms of three *arbitrary* functions of one continuous variable,  $G_T(p), G_L(p)$  and  $\Delta(p)$  with  $p = \sqrt{p^2}$ . Similarly, the vertex  $V_{\mu_1\mu_2\mu_3}(p_1, p_2, p_3)$  (with  $p_{3\mu} = -p_{1\mu} - p_{2\mu}$ ) can be expressed in terms of six independent tensorial structures (see below), each multiplying an undetermined function of the *three* invariants  $p_1^2, p_2^2$ , and  $p_1 \cdot p_2$  (or equivalently  $p_1^2, p_2^2$ , and  $p_3^2$ ).

The challenge is that we are not merely solving for a few numbers, but self-consistently solving for unknown functions of one to three continuous variables.

- The one-loop gluon self-energy diagrams are linearly divergent, and the two-loop gluon self-energy diagrams are individually logarithmically divergent. These divergences must be regulated in a manner which respects gauge invariance,<sup>4</sup> such as dimensional regularization. However since the propagators and vertices appearing in

<sup>4</sup>One might argue that, since the 3PI technique truncated to 3 loops is not gauge invariant, the use of a gauge invariant regulator is unnecessary. But we believe that it is necessary; first, our approach at least retains gauge invariance to low loop order, which would be lost without a gauge invariant regularization. And second, a gauge non-invariant regularization at 1-loop order would allow divergent masses, which fundamentally damage the physics.

the diagrams are general functions of momentum which are presumably only known numerically and only in  $D = 3$  dimensions, we will have to perform these integrations numerically.

The issue of divergences in self-energies is a technical issue which can be handled rather easily in 3 dimensions. The key fact is that at large momenta  $G, \Delta, V$  and  $\mathbb{V}$  approach their free values up to power suppressed corrections. We therefore know the exact form of the UV divergences. If we can find an expression with the same UV divergent behavior which is simple enough to integrate using dimensional regularization, we can add and subtract it. The subtraction renders the numerical integration of the full self-energy expressions finite, while the added version is integrated using dimensional regularization. We will explain this procedure in more detail in the next section.

In order to fit arbitrary functions of one or a few real variables, we will write down a sufficiently flexible *Ansatz* for each function, with some set of variational parameters. That is, we take  $G_T(p) = G_T(c_i, p)$  where  $c_i$  are coefficients – in practice, we take  $G_T(p)$  to be a rational function of  $p$ , and the  $c_i$  are coefficients of this rational function. Extremization of  $\Gamma$  with respect to  $G(p)$  is then replaced by its extremization with respect to the coefficients  $c_i$  of each propagator and vertex function. Under this procedure, some set of integral moments of the Schwinger-Dyson equations will be satisfied, rather than the equations being satisfied at every momentum value. We can determine the quality and limitations of this approach by seeing how the determined correlation functions change as the sizes of the variational *Ansätze* are changed; and we can directly test how well the Schwinger-Dyson equations are obeyed by computing directly the self-energies and vertex corrections at various momenta and comparing to the *Ansatz*, or measuring an integrated mean squared failure of the Schwinger-Dyson equations.

### 3 Divergences and Regularization

As discussed above, variation of  $\Gamma$  with respect to a propagator gives rise to a Schwinger-Dyson equation involving self-energies written in terms of  $G$  and  $V$ . These will be, in general, complicated functions. Yet the self-energies may be UV divergent and so they must be regulated. Even after taming these self-energy divergences, the variation with respect to a propagator or vertex *Ansatz* coefficient  $\delta\Gamma/\delta c_i$  may lead to a divergent integral over the propagator momentum  $p$ . We must also ensure that such divergences do not occur. We will handle these two problems in turn. Throughout we denote the momentum entering a self-energy as  $p$ , and use  $k$  and  $q$  for internal loop momenta.

#### 3.1 Divergences in self-energies

In 3 dimensions the only divergent subdiagrams are gluon self-energies. To handle these divergences we must work in a regularization scheme which renders the self-energy diagrams finite *and* preserves gauge invariance. Therefore we will perform all integrals in dimensional regularization (DR), so  $\int d^3q \rightarrow \int d^Dq$  with  $D = 3 + 2\epsilon$ . Unfortunately the self-energies contain the functions  $G$  and  $V$ , which are complicated and are only known in 3 dimensions.

However, for any integral which is finite and well behaved in 3 dimensions, the  $\epsilon \rightarrow 0$  limit of the DR value is the same as the value directly computed in 3 dimensions. Therefore we will start with identifying the UV divergent behavior of the full integrals containing  $G$  and  $V$  so that we can subtract and add simple integrals with the same divergences. We can then perform the (finite) subtracted versions numerically in 3 dimensions, and finish off by adding back the simple integrals using DR.

Dressed vertices and propagators are well behaved in the IR, hence the only divergences that we expect to see arise from the region of momentum space where  $q$  is large. Therefore we need to determine the asymptotic behaviors of  $G$  and  $V$ . Our theory is superrenormalizable, meaning that the coupling  $g^2$  carries dimension,  $[g^2] = 1 = [q]$ . For large  $q$ ,  $g^2$  is small compared to the relevant scale  $q$ , so the large  $q$  region is weakly coupled and has a perturbative expansion. Further, powers of  $g^2$  in the expansion must be balanced against powers of  $q$  on dimensional grounds. Therefore the leading and first subleading behavior of the propagator in 3 dimensions is

$$G_{\mu\nu}(q) = \frac{1}{q^2} (\mathbf{T}_{\mu\nu}(q) + \xi \mathbf{L}_{\mu\nu}(q)) + \frac{g^2 \Pi^{\text{B}(1)}}{q^3} \mathbf{T}_{\mu\nu}(q) + \mathcal{O}(q^{-4}). \quad (3.1)$$

Similarly, the vertex goes as

$$V \sim q + g^2 q^0 + \mathcal{O}(q^{-1}). \quad (3.2)$$

The specific form of the  $g^2$  correction to  $V$  is known, see Appendix A.3; but as we see in a moment we do not need it here. The one-loop correction to the gluon self-energy is also known. It is purely transverse and equals [25]

$$\Pi_{\mu\nu}^{\text{B}(1)}(q) = q \frac{g^2 N}{64} (\xi^2 + 2\xi + 11) \mathbf{T}_{\mu\nu}(q), \quad (3.3)$$

hence  $\Pi^{\text{B}(1)}$  introduced in Eq. (3.1) is

$$\Pi^{\text{B}(1)} = \frac{N}{64} (\xi^2 + 2\xi + 11). \quad (3.4)$$

Now, consider the diagram

$$\text{Diagram} = \int \frac{d^D q}{(2\pi)^D} V_{\mu\alpha\delta} V_{\nu\beta\kappa} G^{\alpha\beta}(p+q) G^{\delta\kappa}(q), \quad (3.5)$$

where traces over internal color indices are implied (and hence the overall diagram is proportional to the color identity). Expanding the integrand in powers of  $q$ , for  $D = 3$  the large  $q$  region of the integral behaves as

$$\text{Diagram} \sim g^2 \int d^3 q \left[ (q)^2 \frac{1}{(q^2)^2} + \underbrace{2g^2 (q)^2 \frac{\Pi^{\text{B}(1)}}{q^3}}_{\text{NLO propagator}} \frac{1}{q^2} + \underbrace{2g^2 (q)}_{\text{NLO vertex}} \frac{1}{(q^2)^2} + \underbrace{\mathcal{O}(g^4 q^{-4})}_{\text{NLO}^2 + \text{NNLO}} + \dots \right]. \quad (3.6)$$

The first term arises from the leading order (bare) terms in the vertices and propagators, and the next two terms originate from the one-loop corrections (as marked). These first three integrals diverge, so we will have to add and subtract something to cancel their divergent behavior.

Actually, the NLO vertex corrections above will cancel when we sum over the one-loop self-energy corrections. To see this, consider the two diagrams, with one and with two full vertices:

$$\left[ \text{Diagram 1} - \frac{1}{2} \text{Diagram 2} \right]_{q \gg g^2} \sim \frac{1}{2} \text{Diagram 3} \Big|_{q \gg g^2} \quad (3.7)$$

The diagram with one full vertex enters with  $-2$  times the weight of the diagram with two full vertices. Therefore the NLO vertex contributions from these two diagrams cancel, and the UV behavior is the same at NLO as the behavior of a loop with no vertex corrections. Provided that we perform the two diagrams by adding their integrands inside the integration, this cancellation takes place at the level of the integrand and does not lead to a log divergence in the integral in 3 dimensions. (This cancellation does not mean that the NLO vertex correction disappears; instead this correction will be accounted for explicitly when we include two-loop self-energy corrections.)

Next consider the bare part of Eq. (3.6), which is linearly divergent in 3 dimensions. We will add and subtract a diagram made out of the bare vertex and propagator functions,

$$\text{Diagram 4} = g^2 \int_q V_{\mu\alpha\delta}^{(0)} V_{\nu\beta\kappa}^{(0)} G^{(0)\alpha\beta}(p+q) G^{(0)\delta\kappa}(q) \quad (3.8)$$

with  $G^{(0)}$ 's are  $V^{(0)}$ 's denoting bare propagators and vertices. The difference

$$\frac{1}{2} \text{Diagram 5} - \frac{1}{2} \text{Diagram 6} \quad (3.9)$$

is only logarithmically divergent in 3 dimensions. Moreover, Eq. (3.8) is finite when computed in DR and its  $D \rightarrow 3$  limit is

$$\frac{1}{2} \text{Diagram 7} \Big|_{\text{DR}} = p \frac{g^2 N}{64} \left( (\xi^2 + 2\xi + 11) \mathbf{T}_{\mu\nu}(p) - g_{\mu\nu} - \frac{p_\mu p_\nu}{p^2} \right). \quad (3.10)$$

This diagram, plus the bare ghost diagram which cancels the non-transverse piece above, gives rise to  $\Pi^{\text{B}(1)}$  stated earlier.

Lastly, we must subtract something with the same NLO ‘‘propagator’’ behavior remaining in Eq. (3.6). Naively, we could do this by defining

$$G_{\mu\nu}^{(1,\epsilon)}(p) = G_{\mu\alpha}^{(0)}(p) \Pi^{\text{B}(1,\epsilon)\alpha\beta}(p) G_{\beta\nu}^{(0)}(p) = \frac{\Pi^{\text{B}(1,\epsilon)}}{\mu^{2\epsilon}} \frac{1}{p^{3-2\epsilon}} \mathbf{T}_{\mu\nu}(p) \quad (3.11)$$

with  $\Pi_{\alpha\beta}^{\text{B}(1,\epsilon)}(p)$  and  $\Pi^{\text{B}(1,\epsilon)}$  defined by Eqs. (A.8) and (A.9), and then “adding and subtracting” the following diagram:

$$\begin{aligned}
\text{Diagram} &= g^2 \int_q V_{\mu\alpha\delta}^{(0)} V_{\nu\beta\kappa}^{(0)} G^{(0)\alpha\beta}(p+q) G^{(1,\epsilon)\delta\kappa}(q) \\
&= \frac{\mathcal{A}}{\epsilon} g_{\mu\nu} - \frac{\mathcal{B}}{\epsilon} \left( g_{\mu\nu} - \frac{p_\mu p_\nu}{p^2} \right) + \text{finite}.
\end{aligned} \tag{3.12}$$

The problem is that, as the above equation shows, the diagram is not only UV divergent (as expected, with coefficient  $\mathcal{A}$  which we give below), but also IR divergent (with coefficient  $\mathcal{B}$ , whose exact value will not be relevant). If we add and subtract this diagram, we will cause an IR divergence where none should appear. Instead, we will add and subtract an appropriately regulated self-energy corrected propagator,

$$G_{\mu\nu}^{(1,\epsilon)\text{IR Reg}}(p) = \frac{\Pi^{\text{B}(1,\epsilon)}}{\mu^{2\epsilon}} \frac{1}{(p^2 + m^2)^{\frac{3}{2}-\epsilon}} \left( g_{\mu\nu} - \frac{p_\mu p_\nu}{p^2 + m^2} \right) \tag{3.13}$$

so that the integration in

$$\text{Diagram} = g^2 \int_q V_{\mu\alpha\delta}^{(0)} V_{\nu\beta\kappa}^{(0)} G^{(0)\alpha\beta}(p+q) G^{(1,\epsilon)\text{IR Reg}} \delta\kappa(q) \tag{3.14}$$

can still be performed analytically in DR. Upon integration, this diagram has the following form:

$$\text{Diagram} \Big|_{\text{DR}} = \frac{\mathcal{A}}{\epsilon} g_{\mu\nu} + \text{finite}. \tag{3.15}$$

The coefficient that multiplies the UV  $1/\epsilon$ ,

$$\mathcal{A} = -\frac{g^4 N^2}{768\pi^2} \frac{p^{4\epsilon}}{\mu^{4\epsilon}} (\xi + 4)(\xi^2 + 2\xi + 11), \tag{3.16}$$

is identical to that of Eq. (3.12) due to the simple fact that

$$\lim_{q \rightarrow \infty} G_{\mu\nu}^{(1,\epsilon)\text{IR Reg}}(q) = \lim_{q \rightarrow \infty} G_{\mu\nu}^{(1,\epsilon)}(q). \tag{3.17}$$

Naturally, the finite parts of Eq. (3.12) and Eq. (3.14) will differ.

It may worry some readers that we have introduced an IR mass regulator. But we emphasize that we are *not* adding such a regulator to the full propagator  $G^{\mu\nu}(p)$ . We are only adding an IR mass regulator to a term which we add and subtract, for reasons of computational convenience. Hence, the value of the regulator – in fact, the effect of the whole term which we are adding and subtracting – exactly cancels when we combine the

(analytic) result of Eq. (3.14) and the (numerical) result of the full but subtracted diagram in Eq. (3.19). We have naturally checked that the value of the regulator in Eq. (3.13) has no effect on our results for the full self-energy and therefore for the determined value of the full propagator.

Returning to Eq. (3.6), we now have

$$\begin{aligned}
 & \left[ \text{Diagram 1} - \frac{1}{2} \text{Diagram 2} - \frac{1}{2} \text{Diagram 3} - \text{Diagram 4} \right] \\
 & + \left[ \frac{1}{2} \text{Diagram 5} + \text{Diagram 6} \right] \sim \frac{\mathcal{A}}{\epsilon} g_{\mu\nu} + \text{finite} .
 \end{aligned} \tag{3.18}$$

The first line is the only part which contains full propagators; but it is finite at  $D = 3$ . Therefore its value in DR in the  $D \rightarrow 3$  limit simply equals its finite value in 3 dimensions, which we can find by numerical integration. The second line is divergent in 3D but can be carried out relatively easily in DR. It gives rise to the  $\mathcal{A}g_{\mu\nu}/\epsilon$  contribution, and to some of the finite terms presented in Eq. (A.15) (Eq. (A.15) is the sum of Eq. (3.14) as well as a similarly IR regulated Snowcone diagram).

The procedure for handling the 2-loop graphs is similar. While the graphs are more complicated, the procedure is simpler, since in every case the only UV divergences arise when all components of the graph take their bare values. Further, no 2-loop graph we need, when built out of bare quantities, is IR divergent. Therefore we may simply subtract from each 2-loop graph, built using  $G$  and  $V$ , the same graph built using  $G^{(0)}$  and  $V^{(0)}$ . The bare 2-loop graphs can be performed in DR and will also give rise to a  $g_{\mu\nu}/\epsilon$  divergence plus a finite part; the sum of these diagrams is given by Eq. (A.11). In the end, we find that all of the  $1/\epsilon$ 's cancel between two-loop diagrams: the  $\mathcal{O}(g^4)$  IR regulated gluon self-energy is UV finite in DR (the complete expression for which is given by Eqs. (A.11) and (A.15)).

With this procedure in place, the Schwinger-Dyson equation, Eq. (2.8), becomes

$$G^{-1}(p) = G_0^{-1}(p) - \Pi^{(1)}(p) - \Pi^{(2)}(p), \quad (3.19)$$

$$\begin{aligned} \Pi_{\mu\nu}^{(1)} + \Pi_{\mu\nu}^{(2)} = & \text{[Diagram 1]} - \frac{1}{2} \text{[Diagram 2]} + \frac{1}{2} \text{[Diagram 3]} - 2 \text{[Diagram 4]} \\ & + \text{[Diagram 5]} - \frac{1}{2} \text{[Diagram 6]} - \text{[Diagram 7]} - \frac{1}{2} \text{[Diagram 8]} \\ & - \frac{1}{2} \text{[Diagram 9]} + \text{[Diagram 10]} + 2 \text{[Diagram 11]} \\ & + \frac{1}{6} \text{[Diagram 12]} + \frac{1}{2} \text{[Diagram 13]} + \text{[Diagram 14]} + \frac{1}{4} \text{[Diagram 15]} \\ & - 2 \text{[Diagram 16]} - 2 \text{[Diagram 17]} \\ & - \frac{1}{6} \text{[Diagram 18]} - \frac{1}{2} \text{[Diagram 19]} - \text{[Diagram 20]} - \frac{1}{4} \text{[Diagram 21]} \\ & + \text{[Diagram 22]} + 2 \text{[Diagram 23]} \\ & + \Pi_{\mu\nu}^{\text{B}(1,0)}(p) + \lim_{\epsilon \rightarrow 0} \left( \Pi_{\mu\nu}^{\text{B}(2,\epsilon)\text{UV}}(p) + \Pi_{\mu\nu}^{\text{B}(2,\epsilon)\text{IR Reg}}(p) \right). \end{aligned}$$

where the  $\Pi^{\text{B}(a,b)}$ 's represent the sum all bare diagrams computed analytically in dimensional regularization (their values can be read from Appendix. A.1, noting that  $\Pi_{\mu\nu}^{\text{B}(2,\epsilon)\text{IR Reg}}(p)$  is exactly as stated in Eq. (A.15), with no large  $p$  limit taken). In writing this equation we have suppressed the Lorentz indices, as written one should take  $\frac{1}{2} \mathbf{T}_{\mu\nu} \mathbf{\Pi}^{\mu\nu}$  to get the transverse part of the self-energy needed to resum  $G_T$  and  $\mathbf{L}_{\mu\nu} \mathbf{\Pi}^{\mu\nu}$  to get the self-energy needed to resum  $G_L$ .

All ghost self-energies are finite after angular averaging, and the vertex loops are power-counting finite, so no similar subtractions are needed in these cases. Nevertheless, we will still encounter divergences when it comes time to integrate these Schwinger-Dyson

equations over propagator or vertex momenta.

### 3.2 Divergences upon $p$ -integration

Our plan is to find an approximate extremum of  $\Gamma$  by writing variational *Ansätze* for the propagators and vertices and to vary with respect to the *Ansatz* parameters. For instance, one could assume that the transverse propagator  $G_T(p)$  is the sum of a set of test functions with unknown coefficients,  $G_T(p) = \sum_i c_i \phi_i(p)$ . More generally, we choose  $G_T(p)$  to have some functional form with a set of variational parameters  $c_i$ ; we will give our specific choice in Section 4. Then variation of  $\Gamma$  with respect to  $c_j$  would yield

$$\frac{\delta\Gamma}{\delta c_j} = \int d^3p \frac{\delta G_T(p)}{\delta c_j} \frac{\delta\Gamma}{\delta G_T(p)} = \int d^3p \frac{\delta G_T(p)}{\delta c_j} \left( G_T^{-1}(p) - G_T^{(0)-1}(p) + \Pi_T(p) \right), \quad (3.20)$$

and similarly for  $G_L$  and  $\Delta$ . In the last section we ensured that the integrals involved in all self-energies  $\Pi$  are finite. But this does not guarantee that the  $p$  integral above will be finite. For instance, if we chose the *Ansatz*

$$G_T[p, c_i, \text{example}] = \frac{c_1}{p^2 + m^2} + \frac{c_2}{(p^2 + m^2)^{\frac{3}{2}}} + \frac{c_3}{(p^2 + m^2)^2} \quad (3.21)$$

then  $\delta G_T(p)/\delta c_1 = \frac{1}{p^2 + m^2}$ . And if  $c_1 \neq 1$ , then for large  $p$ ,  $G_T^{-1}(p) - G_T^{(0)-1}(p) + \Pi_T(p) \sim p^2$ . In this case Eq. (3.20) would be cubically divergent. Physically this means that if we allow  $G(p)$  to vary from its correct value in a way which does not die away fast in the UV, then  $\Gamma$  will be divergent far from its extremum.

Continuing with the same example, if we fix  $c_1 = 1$ , forcing the propagator to have the correct free-theory limit in the UV, then the most severe UV divergence arises from  $c_2$ . For large  $p$  we have  $\delta G_T(p)/\delta c_2 \sim p^{-3}$  and  $G_T^{-1}(p) - G_T^{(0)-1}(p) + \Pi_T(p) \sim p$  (by virtue of the cancellation of the  $p^2$  terms in  $G_T^{-1}$  and  $G_T^{(0)-1}$ ). In this case the integral is  $\sim \int d^3p (1/p^3)(p)$  which is linearly divergent. This is better but still unacceptable. To ensure a finite answer we must choose an *Ansatz* which automatically enforces the right  $\mathcal{O}(p^2)$  and  $\mathcal{O}(p)$  behavior in  $G_T^{-1}(p)$ , namely,

$$G_T(p) = \frac{1}{p^2} + \frac{g^2 \Pi^{\text{B}(1)}}{p^3} + (\text{Ansatz starting at } \mathcal{O}(p^{-4})). \quad (3.22)$$

In this case,  $\delta G(p)/\delta c_i \lesssim p^{-4}$  automatically, and  $G_T^{-1}(p) - G_T^{(0)-1}(p) + \Pi_T(p) \sim p^0$ . This is sufficient to ensure that the integral in Eq. (3.20) will be UV finite. The same argument applies to  $G_L$  and  $\Delta$ ; in each case we must build in the correct  $1/p^2$  and  $1/p^3$  behavior of the propagator (or  $\mathcal{O}(p^2)$  and  $\mathcal{O}(p)$  behavior in the inverse propagator) into our *Ansatz*; but having done so, the variations  $\delta\Gamma/\delta c_i$  will all automatically be finite (unless there are IR problems).

Applying the same reasoning to the vertices, the variation of  $\Gamma$  with respect to a generic coefficient  $d_i$  determining  $V$  gives rise to a correction of order (the phase space is explained in Appendix B.1)

$$\frac{\delta\Gamma}{\delta d_i} \sim \int p dp q dq k dk \frac{\delta V}{\delta d_i} G(p)G(q)G(k) \left( V - V_{\text{bare}} - \delta V \right). \quad (3.23)$$

If we allow our *Ansatz* to change  $V$  on the scale of its leading behavior  $\sim p, k, q$  then this expression is quadratically divergent. Therefore our *Ansatz* must be restricted such that  $V$  takes on its correct (free) asymptotic limiting behavior. Even so, in this case  $\delta V/\delta d_i$  and  $V - V_{\text{bare}}$  will be  $\mathcal{O}(p^0)$ , giving rise to a log divergence. Therefore we must compute and implement the first subleading behavior of  $V$  and only allow our *Ansatz* to change  $V$  at NNLO,  $\mathcal{O}(p^{-1}, k^{-1}, q^{-1})$ . This will ensure finite variations of  $\Gamma$  with respect to the parameters  $d_i$  (again assuming there are no infrared issues).

It is not necessary to determine the NNLO behavior of either self-energy or vertex corrections in order to avoid potential divergences. This is a good thing, because the  $\mathcal{O}(p^{-4})$  propagator correction (or  $\mathcal{O}(p^0)$  self-energy correction) is where nonperturbative physics first arises. To see this, consider the one-loop self-energy diagram in Eq. (3.5). Let us estimate the contribution when the external momentum  $p$  is large but one of the internal propagators is at a small momentum  $q \sim g^2$ . There is a factor of  $g^2 p^2$  from the vertices,  $1/p^2$  from the hard propagator, and  $\int d^3 q/q^2 \sim q \sim g^2$  from the momentum integration and soft propagator in the soft region. So the contribution when one propagator is soft is of order  $\Pi_{\text{soft}} \sim g^4$ . This contribution is nonperturbative because the behavior of the propagator at small momentum is. Therefore we actually *cannot* determine the NNLO behavior of the propagator at large momenta; the perturbative expansion we alluded to earlier actually fails at this order. Fortunately, determining this order turns out to be unnecessary to eliminate divergences and render our extremization problem well posed.

Note that the elimination of divergences, both in subdiagrams and in the final variation of  $\Gamma$  with respect to variational *Ansatz* parameters, is much easier in  $D = 3$  spacetime dimensions than it would be in  $D = 4$ . In that case, self-energies would be quadratically divergent at all loop orders and  $\delta\Gamma/\delta c_i$  would generically be quartically divergent. It is therefore not completely clear to us how our procedure could be extended to four dimensions without some changes or restrictions. We will not address this issue further at this time.

## 4 Variational *Ansätze*

We will now start to actually solve, rather than discuss, the problem by writing out the variational *Ansätze* used for all propagators and vertices. The only dimensionful constant in 3D Yang-Mills theory is  $g$ . Moreover, a three-loop truncation of  $\Gamma$  only contains planar diagrams, and the only subleading in  $N$  correction which enters when evaluating them is an overall factor of  $(N^2-1)$ ; that is, the coupling and group theory factor for an  $m$ -loop bubble diagram is  $(N^2-1)(g^2 N)^{m-1}$ . Therefore, to the loop order we work, the coupling expansion is strictly an expansion in the 't Hooft coupling  $g^2 N$ . In  $D = 3$  dimensions the 't Hooft coupling has dimensions of energy, and it therefore sets the natural energy scale in the problem. Therefore we will factor out the overall  $(N^2-1)$  and will scale all dimensionful quantities by the appropriate power of  $g^2 N$ , *i.e.*, quantities with dimension  $[\text{mass}]^\alpha$ , are expressed in units of  $(g^2 N)^\alpha$ . For the most part, this eliminates any explicit reference to  $g^2$  or  $N$  in what follows.

Variational coefficients will be generically denoted by  $c_i$ . This is a slight abuse of notation, and one should recall throughout that the  $c_i$  are independent for each function.

For instance, it should not be interpreted from expressions like  $G_T(c_i; p)$  and  $G_L(c_i; p)$  that  $G_T$  and  $G_L$  are defined by the same set of parameters. In practice we will use rational functions (Padé approximants) for our variational *Ansätze*; we distinguish coefficients in numerators from those in denominators by labelling the former by  $a_i$  and the latter by  $b_i$ , so that  $\{c_i\} = \{a_i, b_i\}$  (or  $\{c_i\} = \{a_{ijk}, b_{ijk}\}$  for vertex function coefficients). Finally, it is now always implied that when we refer to a correlation function, we are specifically referring to its *Ansatz*. We will drop the  $c_i$  from the arguments of these functions, so  $G(p)$  implies  $G(c_i; p)$ .

Continuing on,  $G$  is first decomposed into transverse and longitudinal components

$$G^{\mu\nu}(p) = G_T(p)\mathbf{T}^{\mu\nu}(p) + G_L(p)\mathbf{L}^{\mu\nu}(p). \quad (4.1)$$

From the arguments of the previous section, we know that whatever we write down for  $G_T(p)$  has to converge to Eq. (3.22) at large  $p$  (and likewise for  $G_L(p)$  and  $\Delta(p)$ ). Hence,

$$G_T(p) = \frac{1}{p^2 - \Pi_T(p)}, \quad \Pi_T(p) = \mathcal{C}_T^{(1)}p + (\text{Ansatz starting at } \mathcal{O}(p^0)) \quad (4.2)$$

$$G_L(p) = \frac{\xi}{p^2 - \xi\Pi_L(p)}, \quad \Pi_L(p) = \mathcal{C}_L^{(1)}p + (\text{Ansatz starting at } \mathcal{O}(p^0)) \quad (4.3)$$

$$\Delta(p) = \frac{1}{p^2(1 - \Sigma(p)/p^2)}, \quad \Sigma(p)/p^2 = \frac{\mathcal{C}_\Delta^{(1)}}{p + \omega} + (\text{Ansatz starting at } \mathcal{O}(p^{-2})) \quad (4.4)$$

with

$$\mathcal{C}_T^{(1)} = \frac{\xi^2 + \xi + 11}{64}, \quad \mathcal{C}_L^{(1)} = 0, \quad \mathcal{C}_\Delta^{(1)} = \frac{1}{16}. \quad (4.5)$$

We see that  $\mathcal{C}_{T/L/\Delta}^{(1)}$  must be measured in units of  $g^2N$  since  $[\mathcal{C}_{T/L/\Delta}^{(1)}] = [\text{mass}]$ , while  $[G_T] = [\text{mass}]^{-2}$ .

The *Ansatz* for  $\Delta$  differs from  $G_T$  and  $G_L$ ; namely, we assume that  $\Sigma(p) \propto p^2$ , and therefore  $\Delta \propto p^{-2}$ , at small  $p$ . This is a condition which arises due to the structure of ghost vertices, which we will discuss in a little more detail when we present the ghost vertices. The parameter  $\omega$  is not treated as a variational parameter; instead its value is fixed to  $\omega = 1$  (really  $\omega = g^2N$ ). This choice should not be important, provided the variational *Ansatz* is flexible enough.

We will use Padé approximants for the propagator *Ansätze*. The “order” of these *Ansätze* will be denoted by  $N_{\max}^P$ , which refers to the highest power of momentum appearing in the numerator and denominators. With this choice, Eqs. (4.2) - (4.4) read

$$\Pi_T(p) = \mathcal{C}_T^{(1)}p + \Pi_T^{\text{NP}}(p) = \mathcal{C}_T^{(1)}p + \frac{\sum_{i=0}^{N_{\max}^P} a_i^{\{G_T\}} p^i}{\sum_{i=1}^{N_{\max}^P} b_i^{\{G_T\}} p^i + 1} \quad (4.6)$$

$$\Pi_L(p) = \mathcal{C}_L^{(1)}p + \Pi_L^{\text{NP}}(p) = \frac{\sum_{i=0}^{N_{\max}^P} a_i^{\{G_L\}} p^i}{\sum_{i=1}^{N_{\max}^P} b_i^{\{G_L\}} p^i + 1} \quad (4.7)$$

$$\Sigma(p) = \mathcal{C}_\Delta^{(1)}p^2 + \Sigma^{\text{NP}}(p) = \frac{\mathcal{C}_\Delta^{(1)}p^2}{p + \omega} + \frac{\sum_{i=2}^{N_{\max}^P} a_i^{\{\Delta\}} p^i}{\sum_{i=1}^{N_{\max}^P} b_i^{\{\Delta\}} p^i + 1}. \quad (4.8)$$

In each case we define  $\Pi^{\text{NP}}$  as the self-energy minus its one-loop perturbative (linear in momentum) part. In the case of  $\Sigma$  this is *not* the same as the part determined by the variational *Ansatz*.

In constructing the most general gluon 3-vertex  $V$  (where it is assumed that momentum flows out of a vertex), six independent tensor structures require consideration. We will adopt the basis used in Refs. [28, 29], which is

$$\begin{aligned}
\mathbf{A}_{\mu_1\mu_2\mu_3} &= g_{\mu_1\mu_2}(p_1 - p_2)_{\mu_3} \\
\mathbf{B}_{\mu_1\mu_2\mu_3} &= g_{\mu_1\mu_2}(p_1 + p_2)_{\mu_3} \\
\mathbf{C}_{\mu_1\mu_2\mu_3} &= [p_1 \cdot p_2 g_{\mu_1\mu_2} - p_{1\mu_2} p_{2\mu_1}](p_1 - p_2)_{\mu_3} \\
\mathbf{F}_{\mu_1\mu_2\mu_3} &= [p_1 \cdot p_2 g_{\mu_1\mu_2} - p_{1\mu_2} p_{2\mu_1}] [(p_2 \cdot p_3) p_{1\mu_3} - (p_1 \cdot p_3) p_{2\mu_3}] \\
\mathbf{H}_{\mu_1\mu_2\mu_3} &= g_{\mu_1\mu_2} [(p_1 \cdot p_3) p_{2\mu_3} - (p_2 \cdot p_3) p_{1\mu_3}] + \frac{1}{3} (p_{1\mu_3} p_{2\mu_1} p_{3\mu_2} - p_{1\mu_2} p_{2\mu_3} p_{3\mu_1}) \\
\mathbf{S}_{\mu_1\mu_2\mu_3} &= p_{1\mu_3} p_{2\mu_1} p_{3\mu_2} + p_{1\mu_2} p_{2\mu_3} p_{3\mu_1}.
\end{aligned} \tag{4.9}$$

Color dependence can be factored out of the vertex function,

$$V_{\mu_1\mu_2\mu_3}^{a_1 a_2 a_3}(p_1, p_2, p_3) = F^{a_1 a_2 a_3} V_{\mu_1\mu_2\mu_3}(p_1, p_2, p_3) \tag{4.10}$$

where  $F^{abc} = -if_{abc}$  is the adjoint representation matrix, satisfying  $F^{iab} F^{jba} = C_A \delta^{ij}$ ,  $C_A = N$  for  $\text{SU}(N)$ . In a similar fashion to the propagators, our *Ansatz* for  $V$  is designed so that it can be easily made to converge to its perturbative form at large momenta. We will separate the various contributions to  $V$  much like we did with the propagators,

$$V_{\mu_1\mu_2\mu_3} = g(V_{\mu_1\mu_2\mu_3}^{(0)} + V_{\mu_1\mu_2\mu_3}^{(1)} + V_{\mu_1\mu_2\mu_3}^{\text{NP}}). \tag{4.11}$$

The bare and one-loop corrections are denoted by  $V^{(0)}$  and  $V^{(1)}$ , while  $V^{\text{NP}}$  denotes the nonperturbative correction to the vertex that has to be solved for self-consistently by finding the stationary point of  $\Gamma$ . The bare term,  $V^{(0)}$  is simply

$$V_{\mu_1\mu_2\mu_3}^{(0)} = (p_2 - p_3)_{\mu_1} g_{\mu_2\mu_3} + (p_3 - p_1)_{\mu_2} g_{\mu_1\mu_3} + (p_1 - p_2)_{\mu_3} g_{\mu_1\mu_2} \tag{4.12}$$

which is expressed entirely in terms of cyclic permutations of the  $\mathbf{A}$  tensor, *i.e.*

$$V_{\mu_1\mu_2\mu_3}^{(0)} = A^{(0)} \mathbf{A}_{\mu_1\mu_2\mu_3} + \text{cyclic perms.} \tag{4.13}$$

with  $A^{(0)} = 1$ . The one-loop correction to the vertex  $V^{(1)}$  has a much more intricate tensor structure

$$\begin{aligned}
V_{\mu_1\mu_2\mu_3}^{(1)}(p_1, p_2, p_3) &= A^{(1)}(p_1, p_2; p_3) \mathbf{A}_{\mu_1\mu_2\mu_3} + B^{(1)}(p_1, p_2; p_3) \mathbf{B}_{\mu_1\mu_2\mu_3} \\
&+ C^{(1)}(p_1, p_2; p_3) \mathbf{C}_{\mu_1\mu_2\mu_3} + F^{(1)}(p_1, p_2; p_3) \mathbf{F}_{\mu_1\mu_2\mu_3} \\
&+ H^{(1)}(p_1, p_2, p_3) \mathbf{H}_{\mu_1\mu_2\mu_3} + S^{(1)}(p_1, p_2, p_3) \mathbf{S}_{\mu_1\mu_2\mu_3} \\
&+ \text{cyclic perms.}
\end{aligned} \tag{4.14}$$

and likewise for  $V^{\text{NP}}$ . As we discussed above, we need the explicit forms of the 1-loop vertex corrections in order to eliminate logarithmic UV divergences in the variational problem.

We present explicit results for the 1-loop vertices in Appendix A.3 and we use those results in the following<sup>5</sup>. Note in particular that  $S^{(1)} = 0$ . However it remains to write variational *Ansätze* for  $V^{\text{NP}}$ . Here we make no assumptions about the vanishing of the coefficients for any of the tensorial structures. The functions  $A$ ,  $C$  and  $F$  are symmetric in their first two arguments,  $B$  is antisymmetric in its first two arguments,  $H$  is fully symmetric and  $S$  is fully antisymmetric. We respect these symmetry properties by choosing the following *Ansätze*:

$$A^{\text{NP}}(p_1, p_2; p_3) = \frac{1}{p_1^2 + p_2^2 + p_3^2 + \omega^2} \frac{\sum_{i \geq j} a_{ijk}^{\{A\}} (p_1^i p_2^j + p_1^j p_2^i) p_3^k}{\sum_{i \geq j} b_{ijk}^{\{A\}} (p_1^i p_2^j + p_1^j p_2^i) p_3^k} \quad (4.15)$$

$$B^{\text{NP}}(p_1, p_2; p_3) = \frac{1}{p_1^2 + p_2^2 + p_3^2 + \omega^2} \frac{\sum_{i > j} a_{ijk}^{\{B\}} (p_1^i p_2^j - p_1^j p_2^i) p_3^k}{\sum_{i \geq j} b_{ijk}^{\{B\}} (p_1^i p_2^j + p_1^j p_2^i) p_3^k} \quad (4.16)$$

$$C^{\text{NP}}(p_1, p_2; p_3) = \frac{1}{p_1^4 + p_2^4 + p_3^4 + \omega^4} \frac{\sum_{i \geq j} a_{ijk}^{\{C\}} (p_1^i p_2^j + p_1^j p_2^i) p_3^k}{\sum_{i \geq j} b_{ijk}^{\{C\}} (p_1^i p_2^j + p_1^j p_2^i) p_3^k} \quad (4.17)$$

$$F^{\text{NP}}(p_1, p_2; p_3) = \frac{1}{p_1^6 + p_2^6 + p_3^6 + \omega^6} \frac{\sum_{i \geq j} a_{ijk}^{\{F\}} (p_1^i p_2^j + p_1^j p_2^i) p_3^k}{\sum_{i \geq j} b_{ijk}^{\{F\}} (p_1^i p_2^j + p_1^j p_2^i) p_3^k} \quad (4.18)$$

$$H^{\text{NP}}(p_1, p_2, p_3) = \frac{1}{p_1^4 + p_2^4 + p_3^4 + \omega^4} \frac{\sum_{i \geq j \geq k} a_{ijk}^{\{H\}} (p_1^i p_2^j p_3^k + \text{perms.})}{\sum_{i \geq j \geq k} b_{ijk}^{\{H\}} (p_1^i p_2^j p_3^k + \text{perms.})} \quad (4.19)$$

$$S^{\text{NP}}(p_1, p_2, p_3) = \frac{1}{p_1^4 + p_2^4 + p_3^4 + \omega^4} \frac{\sum_{i > j > k} a_{ijk}^{\{S\}} (\epsilon_{xyz} p_x^i p_y^j p_z^k)}{\sum_{i \geq j \geq k} b_{ijk}^{\{S\}} (p_1^i p_2^j p_3^k + \text{perms.})} \quad (4.20)$$

which automatically have these symmetries built into them ( $\epsilon_{xyz}$  is the permutation symbol). Each sum is truncated so that  $(i+j+k) \leq N_{\text{max}}^{\text{V}}$ .

Notice that not all six tensors are of the same dimension;  $\mathbf{A}$  and  $\mathbf{B}$  have dimensions of [mass],  $\mathbf{C}$ ,  $\mathbf{H}$  and  $\mathbf{S}$  are [mass]<sup>3</sup> and  $\mathbf{F}$  is [mass]<sup>5</sup>. In every case the UV behavior of the vertex function must satisfy  $V^{(1)} \propto 1$  and  $V^{\text{NP}} \propto p^{-1}$ . We enforce the correct momentum scaling for the vertex functions by hand, so that the Padé Approximants are all  $\mathcal{O}(1)$ ; this way, despite the individual dimensionalities of the Vertex functions, all of the *Ansätze* are the same “size.”

The ghost-gluon vertex  $\mathbb{V}$  is somewhat simpler. Factoring out explicit color dependence,

$$\mathbb{V}_{\mu_3}^{a_1 a_2 a_3}(p_1, p_2, p_3) = g F^{a_1 a_2 a_3} \mathbb{V}_{\mu_3}(p_1, p_2, p_3) \quad (4.21)$$

with the outgoing ghost and gluon indexed by  $(a_1, p_1)$  and  $(a_3, \mu_3, p_3)$  respectively ( $p_1$  flows outwards), we have

$$\mathbb{V}_{\mu_3}(p_1, p_2, p_3) = \mathbb{A}(p_1, p_2, p_3) p_{1\mu_3} + \mathbb{B}(p_1, p_2, p_3) p_{2\mu_3}, \quad (4.22)$$

---

<sup>5</sup>Setting  $\omega^{(1)} = 1/4$ ; this parameter serves an analogous purpose to  $\omega$  as it appears in the ghost propagator, see Eq. (A.35).

where

$$\mathbb{A}(p_1, p_2, p_3) = \mathbb{A}^{(0)} + \mathbb{A}^{(1)} + \mathbb{A}^{\text{NP}} \quad (4.23)$$

$$\mathbb{B}(p_1, p_2, p_3) = \mathbb{B}^{(1)} + \mathbb{B}^{\text{NP}}, \quad (4.24)$$

and

$$\mathbb{A}^{\text{NP}} = \frac{1}{p_1^2 + p_2^2 + p_3^2 + \omega^2} \frac{\sum a_{ijk}^{\{\mathbb{A}\}} p_1^i p_2^j p_3^k}{\sum b_{ijk}^{\{\mathbb{A}\}} p_1^i p_2^j p_3^k} \quad (4.25)$$

$$\mathbb{B}^{\text{NP}} = \frac{1}{p_1^2 + p_2^2 + p_3^2 + \omega^2} \frac{p_1 \sum a_{ijk}^{\{\mathbb{B}\}} p_1^i p_2^j p_3^k + (p_2 - p_3) \sum a_{ij}^{\{\mathbb{B}\}} p_2^j p_3^k}{\sum b_{ijk}^{\{\mathbb{B}\}} p_1^i p_2^j p_3^k} \quad (4.26)$$

In this case  $\mathbb{A}^{(0)} = 1$ , and as above,  $\mathbb{A}^{(1)}$  and  $\mathbb{B}^{(1)}$  are one-loop corrections (read directly from Eqs. (A.36) and (A.37), modulo  $g^2 N$ ).

The *Ansatz* for  $\mathbb{B}$  is chosen so as to guarantee that  $\lim_{p_1 \rightarrow 0} \mathbb{B} = 0$ , linearly in  $p_1$ . Let us briefly discuss this assumption, and our similar assumption that the ghost self-energy  $\Sigma(p) \propto p^2$  at small  $p$ . Both properties arise because the tree-level ghost vertex  $\mathbb{V}_\mu^{(0)}(p_1, p_2, p_3) \propto p_{1\mu}$  the outgoing ghost momentum. In any loop diagram modifying  $\mathbb{V}$ , with arbitrarily many loops, the outgoing ghost line, with momentum  $p_1$ , always encounters a bare  $\mathbb{V}$ , leading to a proportionality of the full diagram to  $p_1$ . This proportionality is automatic in the  $\mathbb{A}$  term; we are also enforcing it in the  $\mathbb{B}$  term. One could argue that this argument assumes a strict diagrammatic expansion and might be violated somehow when we fully resum. However, it is at least self-consistent that  $\mathbb{B} \propto p_1$  (note that  $\lim_{p_1 \rightarrow 0} (p_2 - p_3) = 0$  linearly in  $p_1$ ). And if it is, this is enough to ensure that any vertex correction, with resummed as well as bare vertices, is still always proportional to  $p_1$ . Since the vertices are always proportional to  $p_1$ , the self-energy must also vanish at least linearly in  $p$ ; but assuming that  $\Sigma(p)$  is smooth at small  $p$  (which is true provided that there are no IR divergences in ghost self-energy corrections),  $\Sigma(p)$  must in fact vanish quadratically in  $p$ . Building these properties into our *Ansätze* improves the stability of the numerical extremization; however we have also tried to solve the variational problem without these assumptions (using *Ansätze* which allow  $\mathbb{B} \propto p_1^0$  and  $\Sigma(p) \propto p^0$ ), with results which are consistent with the assumed  $\propto p_1$  and  $\propto p^2$  behaviors.

#### 4.1 Numerical Implementation

Obtaining the solution in terms of the variational coefficients involves performing three non-trivial tasks, which together can be referred to as the numerical implementation. These tasks are

- Tensor contraction and diagram generation
- Numerical integration over a 9D phase-space (three loops)
- Using an extremization algorithm to locate the extremum of  $\Gamma$ .

Concerning diagram generation, the purely gluonic *Mercedes-Benz* is by far the most complicated diagram. Each propagator has 2 tensorial structures, each vertex has 14 (the permutations of the 6 structures described in the last subsection). An inefficient tensor contraction would therefore contain  $2^6 14^4 = 2458624$  terms. Therefore it is important to perform the tensorial contractions carefully, building intermediate structures with the minimum number of terms. For instance, the *Mercedes-Benz* can be regarded as

The diagram shows a Mercedes-Benz diagram (a central vertex with three internal lines forming a triangle) on the left, followed by an equals sign, then a vertex diagram (a central vertex with two external lines and one internal line) in the middle, followed by a multiplication sign, then a triangle diagram (a triangle with three internal lines) on the right, and a comma. The equation is labeled (4.27).

which we will write as *vertex* contracted with *triangle*. The *triangle* can be represented in terms of a basis of 36 tensors (all three-index objects that can be constructed out of three momenta [two external and one loop] and the metric), and likewise, the resummed vertex contains 14 distinct tensors (all three-index objects that can be constructed out two momenta and the metric, due to momentum conservation). Specifically, the vertex *after* contracting the tensors associated with the propagators is of form

$$\begin{aligned}
V_{\mu_1\mu_2\mu_3} = & Z_{001}g_{\mu_1\mu_2}p_{1\mu_3} + Z_{010}g_{\mu_1\mu_3}p_{1\mu_2} + Z_{100}g_{\mu_2\mu_3}p_{1\mu_1} \\
& + Z_{002}g_{\mu_1\mu_2}p_{2\mu_3} + Z_{020}g_{\mu_1\mu_3}p_{2\mu_2} + Z_{200}g_{\mu_2\mu_3}p_{2\mu_1} \\
& + Z_{112}p_{1\mu_1}p_{1\mu_2}p_{2\mu_3} + Z_{121}p_{1\mu_1}p_{2\mu_2}p_{1\mu_3} + Z_{211}p_{2\mu_1}p_{1\mu_2}p_{1\mu_3} + Z_{111}p_{1\mu_1}p_{1\mu_2}p_{1\mu_3} \\
& + Z_{221}p_{2\mu_1}p_{2\mu_2}p_{1\mu_3} + Z_{212}p_{2\mu_1}p_{1\mu_2}p_{2\mu_3} + Z_{122}p_{1\mu_1}p_{2\mu_2}p_{2\mu_3} + Z_{222}p_{2\mu_1}p_{2\mu_2}p_{2\mu_3}. \quad (4.28)
\end{aligned}$$

With the *vertex* and *triangle* factored as such, standard algebraic packages can perform all of the remaining tensor contractions and simplifications.

In addition to drastically simplifying diagram construction, the use of these bases allows for an economical use of floating point operations. The *triangle* is contained in all gluonic derivatives of  $\Gamma$ ; furthermore, the 36 *triangle*  $Z$ -coefficients are by far the largest polynomials contained within the problem. With the triangle expressed as such, each of these 36 functions need only to be computed a single time at each point in a 6D space of integration variables. This is important because high-dimensional numerical integration will require of order  $10^5$  evaluations of each diagram *per step* in the extremization procedure for  $\Gamma$ .

With the Lorentz algebra in hand, we turn to the problem of multidimensional numerical integration. The first step is to choose a convenient basis for integration. Our choice is described in Appendix B. Performing the global (Eulerian) angular integrations, two-loop diagrams require a 3D integration and three-loop integrals require a 6D integration. These happen to be the same as the number of propagators in the bubble diagrams built with 3-point vertices. And it is possible, and convenient, to choose integration variables which are precisely the magnitudes of the momenta on each propagator. (This is a special feature of phase space integration in 3 dimensions, discussed in the appendix.) The most numerically challenging integration is again the *Mercedes-Benz* topology. In the notation of Appendix B, the three finite-range (angular) integrations, over  $k'$ ,  $q'$ , and  $l$ , as well as

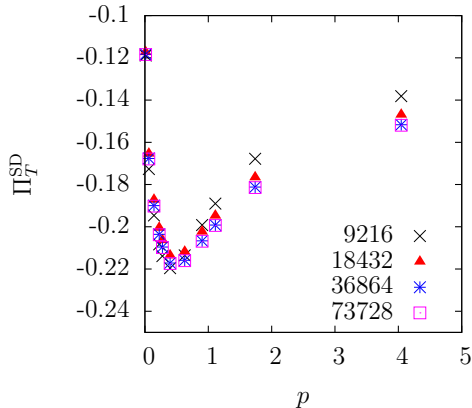


**Figure 3.** Non-perturbative correction to  $\Pi_T$ , viz. Eq. (4.29), as a function of the total number of integration points along the  $k$ ,  $q$ ,  $k'$ ,  $q'$  and  $l$  integration axes (labelled in the bottom right corner).

the  $p$  integration, were performed using Gaussian quadratures, while the (infinite)  $k$  and  $q$  momentum axes were rescaled into the unit interval and sampled using an array of points constructed with a quasi-random hopping Halton series.<sup>6</sup> Our quadratures procedure is symmetric over intervals, which ensures that certain cancellations on angular integration are preserved, and it avoids edgepoint evaluations. Also, since neither algorithm uses random or pseudorandom numbers or dynamic mesh refinement, each integration evaluation is over exactly the same distribution of phase-space points. This ensures that the effective action  $\Gamma$  is not “noisy” in the sense that it does not fluctuate between evaluations with the same or almost the same choices of propagator and vertex functions, a feature which is essential for conjugate-gradient and other differential extremum seeking algorithms.

To test the stability of our algorithm against changes in the number of integration points, we computed the 2-loop self-energy for particular values of full propagators and vertices with varying numbers of integration points. As illustrated in Fig. 3, the results converge when sufficiently many integration points are used. Finally, as an additional check, our numerical procedure for performing 3-loop integrals was tested against the known result for the bare massive 3-loop *Mercedes-Benz* in 3D [30], with which we find agreement.

Now that we have explained how numerical integrations can be performed, we turn to the problem of extremizing the effective action  $\Gamma$ . One challenge is that, because of gauge fixing and ghosts, the extremum is actually a saddle, rather than a maximum or minimum. This can be easily seen from the first line of Eq. (2.6), where the gluon propagator  $G$  and the ghost propagator  $\Delta$  enter with opposite sign. With the sign conventions chosen there, the extremum of the 1-loop action with respect to  $G$  is a maximum; with respect

<sup>6</sup>More specifically, we first write  $k = px/(1-x)$  with  $x \in [0, 1)$ . Then we write  $x = 3y^2 - 2y^3$  with  $y \in [0, 1)$  chosen with uniform weight. The former transformation ensures that  $k, q, p$  are of comparable magnitude; the latter transformation increases the sampling at the top and bottom relative to the middle of the range.

to  $\Delta$  it is a minimum. This rules out any straightforward application of the conjugate gradient algorithm. The Newton-Raphson algorithm can find general extrema, but it is inefficient and tends to converge well only in rather small basins of attraction. So some hybrid approach is needed.

Fortunately, despite it being not at all *a priori* obvious, one observes for the most part that each individual function that makes up the extremization problem has relatively little effect on the others. This opens up the possibility of iteratively extremizing each constituent function ( $G$ ,  $\Delta$ ,  $V$  and  $\mathbb{V}$ ). Our procedure was to start with vertices set to their 1-loop values and propagators set to some naive initial guess. Then we perform a conjugate gradient extremization with respect to  $G$ , then a conjugate gradient extremization with respect to  $\Delta$  (with opposite sign on the gradient).<sup>7</sup> Iteratively extremizing  $G$  and  $\Delta$  solves the 3-loop 2PI problem. Then we use gradient descent to extremize  $\Gamma$  with respect to the three-gluon vertex functions. Finally, the ghost vertex corrections are improved using the Newton-Raphson method. Then the procedure is iterated (propagators and gluon vertices, then ghost vertices) until convergence is achieved.

The convergence of the algorithm, when applied to the 3-loop 2PI problem in Landau gauge, is depicted in Fig. 4. The figure compares the *Ansatz* value for the self-energies,  $\Pi_T^{\text{NP}}$  and  $\Sigma^{\text{NP}}$  as defined in Eq. (4.6), Eq. (4.8), to the values directly evaluated by summing the self-energy diagrams,  $\Pi_T^{\text{SD}}$  and  $\Sigma^{\text{SD}}$ ; in each case we have removed the 1-loop linear-in- $p$  contribution. That is,

$$\Pi_T^{\text{SD}} \equiv \mathbf{T}^{\mu\nu}(\Pi_{\mu\nu}^{(1)} + \Pi_{\mu\nu}^{(2)})/(\text{D} - 1) - \mathcal{C}_T^{(1)}p, \quad (4.29)$$

and similarly for  $\Sigma^{\text{SD}}$ . The extremization procedure for the effective action with respect to one of the variational coefficients in  $G_T$ , Eq. (3.20), then corresponds to

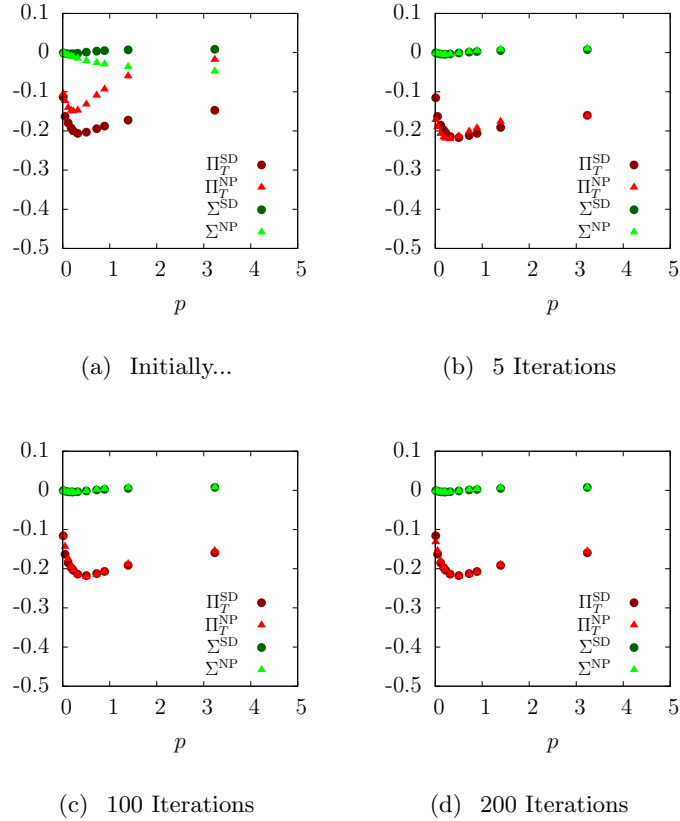
$$\frac{\delta\Gamma}{\delta c_j} = \frac{(\text{D} - 1)(N^2 - 1)}{2} \int \frac{d^3p}{(2\pi)^3} \frac{\delta G_T(p)}{\delta c_j} (-\Pi_T^{\text{NP}}(p) + \Pi_T^{\text{SD}}(p)). \quad (4.30)$$

Fig. 4 shows two things. First, even though the initial guess for the self-energy falls quite far off the actual value, after relatively few iterations the fitted and true values of the self-energy become similar, and the eventual convergence is excellent. Second, the value of the self-energy  $\Pi_T^{\text{SD}}$  actually depends quite weakly on precise form of  $\Pi_T^{\text{NP}}(p)$ . That is why our procedure of varying  $\Gamma$  with respect to individual functions (rather than trying to do everything at once) works so effectively. The presence of vertices definitely makes matters more complicated; however, it is also observed that  $\Pi_T^{\text{SD}}(p)$  is fairly insensitive to their inclusion.

Eq. (4.30) should be interpreted as an Euler-Lagrange type of equation for  $\Pi$ , and a vertex analogue can be defined as follows. For instance when  $c_i$  belongs to the gluon

---

<sup>7</sup>In practice we also accelerate this procedure as follows. We evaluate the self-energy diagrams  $\Pi(p)$  at a sample of  $p$  values holding  $G$  fixed. Then we conjugate-gradient extremize  $G$  in Eq. (3.20) but treating the self-energy  $\Pi$  as fixed. We insert the new value of  $G$  into the evaluation of the self-energy and iterate. This minimizes the number of evaluations of  $\Pi(p)$ , the most numerically expensive part of the procedure, needed to converge to the extremum. But the extremum obtained by this procedure is the one which satisfies Eq. (3.20), as desired.



**Figure 4.** Evolution of the self-energy under the gradient descent algorithm. Here  $\Pi^{\text{NP}}$  is the nonperturbative self-energy according to the *Ansatz*, while  $\Pi^{\text{SD}}$  is the value as determined by evaluating the self-energy diagrams. As the algorithm is iterated, the *Ansatz* approaches a correct reproduction of the self-energy.

$H$ -function, the variation of  $\Gamma$  takes on the following form

$$\frac{\delta\Gamma}{\delta c_j} = \int \frac{d^3p}{(2\pi^3)} \frac{d^3k}{(2\pi)^3} \frac{\delta H^{\text{NP}}(p, k, x)}{\delta c_j} (-\mathbf{H} \cdot V^{\text{NP}}(p, k, x) + \mathbf{H} \cdot V^{\text{SD}}(p, k, x)), \quad (4.31)$$

with

$$\mathbf{H} \cdot V^{\text{NP}}(p, k, x) \equiv -(N^2 - 1) \mathbf{H}_{\mu_1\mu_2\mu_3} G^{\mu_1\nu_1}(p) G^{\mu_2\nu_2}(k) G^{\mu_3\nu_3}(x) \left( \frac{1}{6} V_{\nu_1\nu_2\nu_3} - \frac{1}{6} V_{\nu_1\nu_2\nu_3}^{(0)} \right), \quad (4.32)$$

where the overall minus sign comes from the ordering of color indices.  $\mathbf{H} \cdot V^{\text{SD}}(p, k, x)$  is defined in a similar manner, except that the term in brackets in Eq. (4.32) contains all of the higher loop terms in the vertex Schwinger-Dyson equation, Eq. (2.9). The values of  $\mathbf{H} \cdot V^{\text{SD}}(p, k, x)$  and  $\mathbf{H} \cdot V^{\text{NP}}(p, k, x)$  along the curve defined by  $k = p/4$  and  $\cos \theta_{pk} = 1/4$  are plotted in Fig. 5. Fig. 6 contains plots of a similarly defined set of quantities related to the ghost vertex.

The *Ansätze* in Figs. 4 - 6 correspond to  $N_{\text{max}}^{\text{P}} = 3$  and  $N_{\text{max}}^{\text{V}} = 3$ , from which we observe that the solution is well described by third order Padés. However, the size of the

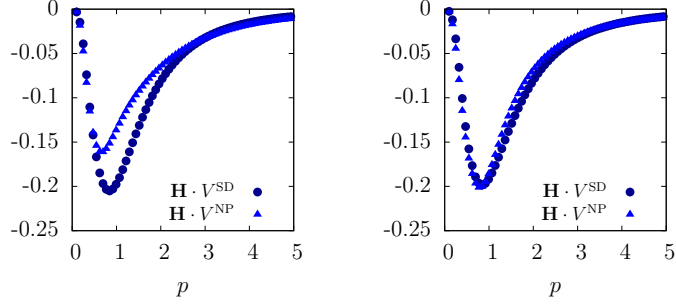


**Figure 5.** Vertex analog of Fig. 4 in Landau gauge, illustrating in this case, convergence of the  $H$ -function (see Eq. (4.31)) and the gluon vertex as a whole. The values reside on the curve  $k = p/4$  and  $\cos \theta_{pk} = 1/4$ . The figure on the left corresponds to  $H^{\text{NP}} = 0$ , whereas the figure on the right corresponds to  $H^{\text{NP}}$  which extremizes  $\Gamma$ . Note that the basis, Eq. (4.9), used for the vertex is not orthogonal, so  $H^{\text{NP}} = 0$  does not imply that  $\mathbf{H} \cdot \mathbb{V}^{\text{NP}} \neq 0$ , as illustrated here.

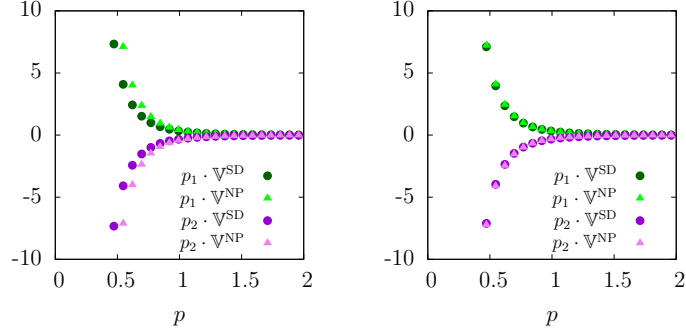


**Figure 6.** Convergence of the ghost-gluon vertex functions in Landau gauge; similar to Fig. 5, the figure on the left corresponds to an initial guess of  $\mathbb{V}^{\text{NP}} = 0$ , whereas that on the right corresponds to the “solution” for  $\mathbb{V}^{\text{NP}}$  which extremizes  $\Gamma$ .

*Ansätze* can have a major effect on the outcome of this technique. With too few coefficients, the numerics are much simpler, but one is not able to obtain the correct final answer. However, as the number of coefficients increases, the problem becomes very numerically difficult (considering the relative ease with which poles may form in the denominators of the Padé approximants), and furthermore, the data will eventually be over-fitted. We find that at  $N_{\text{max}}^{\text{P}} = 3$  and  $N_{\text{max}}^{\text{V}} = 3$  the problem is still not overly difficult to solve, despite there being a total of 174 coefficients in Landau gauge (with an additional 33 in other gauges). At the same time we are not over-fitting. This choice is further motivated by the general shape of functions we are attempting to converge to; the presence of additional “wiggles” would necessitate larger *Ansätze*.

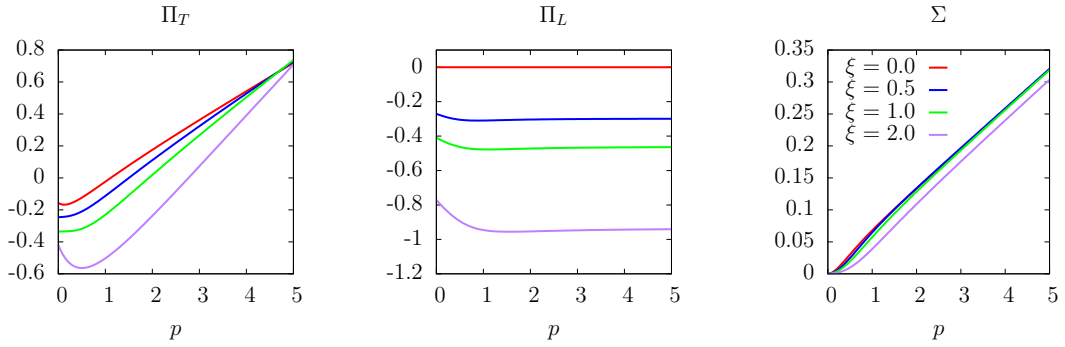


**Figure 7.** Self-energies.

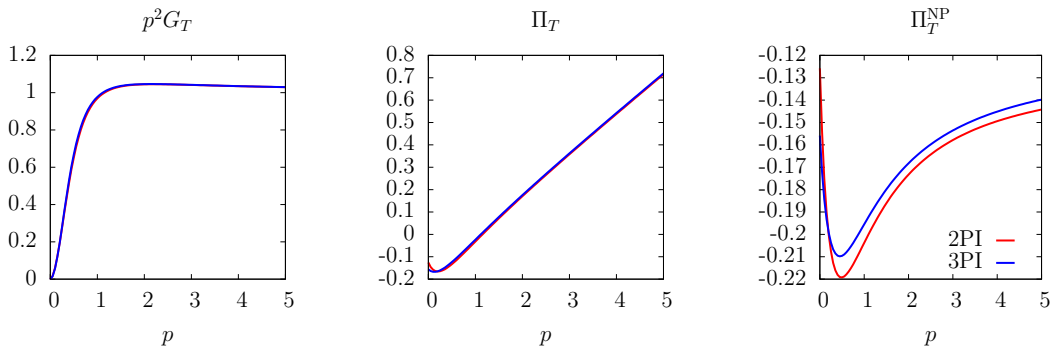


**Figure 8.** Comparison between the 2PI (bare vertices only) and 3PI (vertices included) solutions. The correction to  $G_T$  that we obtain when including the vertices is indeed small (in Landau gauge).

## 5 Results

The extremization procedure was carried out for several choices of the gauge parameter  $\xi$ , namely 0.0, 0.5, 1.0 and 2.0. The resulting self-energies are shown in Fig. 7, and the gluon three-vertex functions  $A$  through  $S$  and the ghost three-point functions  $\mathbb{A}^{\text{NP}}$  and  $\mathbb{B}^{\text{NP}}$  are plotted in Fig. 9, which shows the Landau gauge results, and Fig. 10, which shows the results in Feynman gauge. The Landau gauge variational coefficients are stated in Table 2. The results for  $\xi = 0.5$  and  $\xi = 2.0$  are qualitatively similar.

In Landau gauge,  $G_L$  is zero, so it is not included in the variation; hence  $G_L$  and  $\Pi_L$  are depicted as zero in the plots. Furthermore, when the tensorial structure  $\mathbb{B}_{\mu_1\mu_2\mu_3}$  is contracted against transverse propagators on all three legs, the result is zero; therefore the coefficient  $B$  vanishes exactly in Landau gauge, though not in gauges with nonzero  $\xi$ . The function  $S$  turns out to vanish in all gauges.

The effect of including the vertices and allowing them to vary is shown in Fig. 8, where we see a comparison between the 2PI and 3PI solutions. The inclusion of the vertices only has a slight effect the resulting propagators.

The dependence of  $G$ ,  $V$ , *etc.* on the choice of the gauge fixing parameter  $\xi$  does not

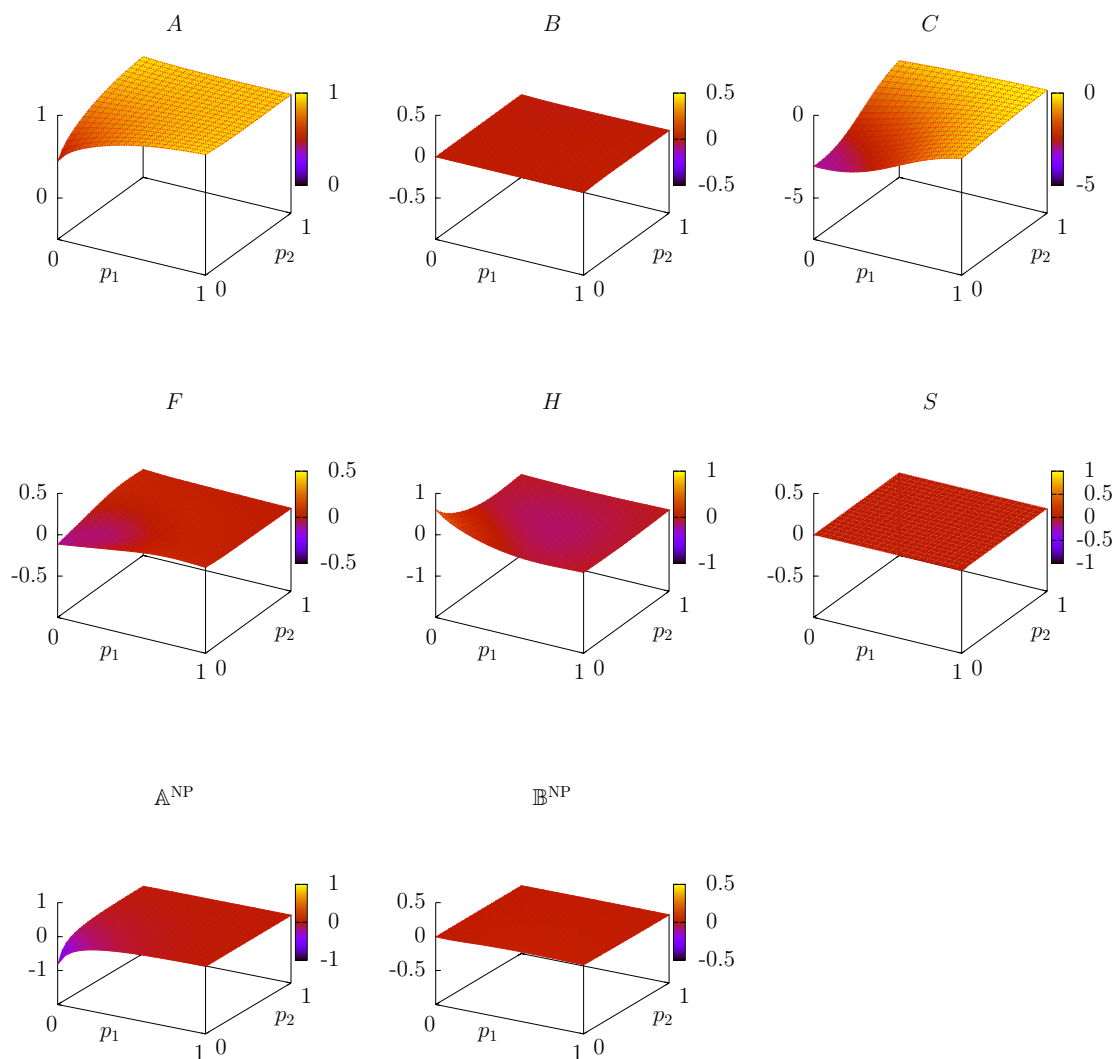


**Figure 9.**  $\xi = 0.0$ ,  $N_{\max}^{\text{P}} = 3$ ,  $N_{\max}^{\text{V}} = 3$ ,  $\cos \theta_{p_1, p_2} = 1/4$ .

by itself indicate a breakdown or limitation on the 3PI approach. The relevant question is, how dependent are gauge independent quantities on  $\xi$ , and how closely do such quantities correspond to the nonperturbative values determined, for instance, using lattice techniques? Any  $\xi$  dependence in gauge invariant quantities would be an ambiguity, and any error in their value in comparison to lattice determinations would be a failure, of the 3PI technique. Such comparisons are essential, but they are beyond the scope of the present manuscript.

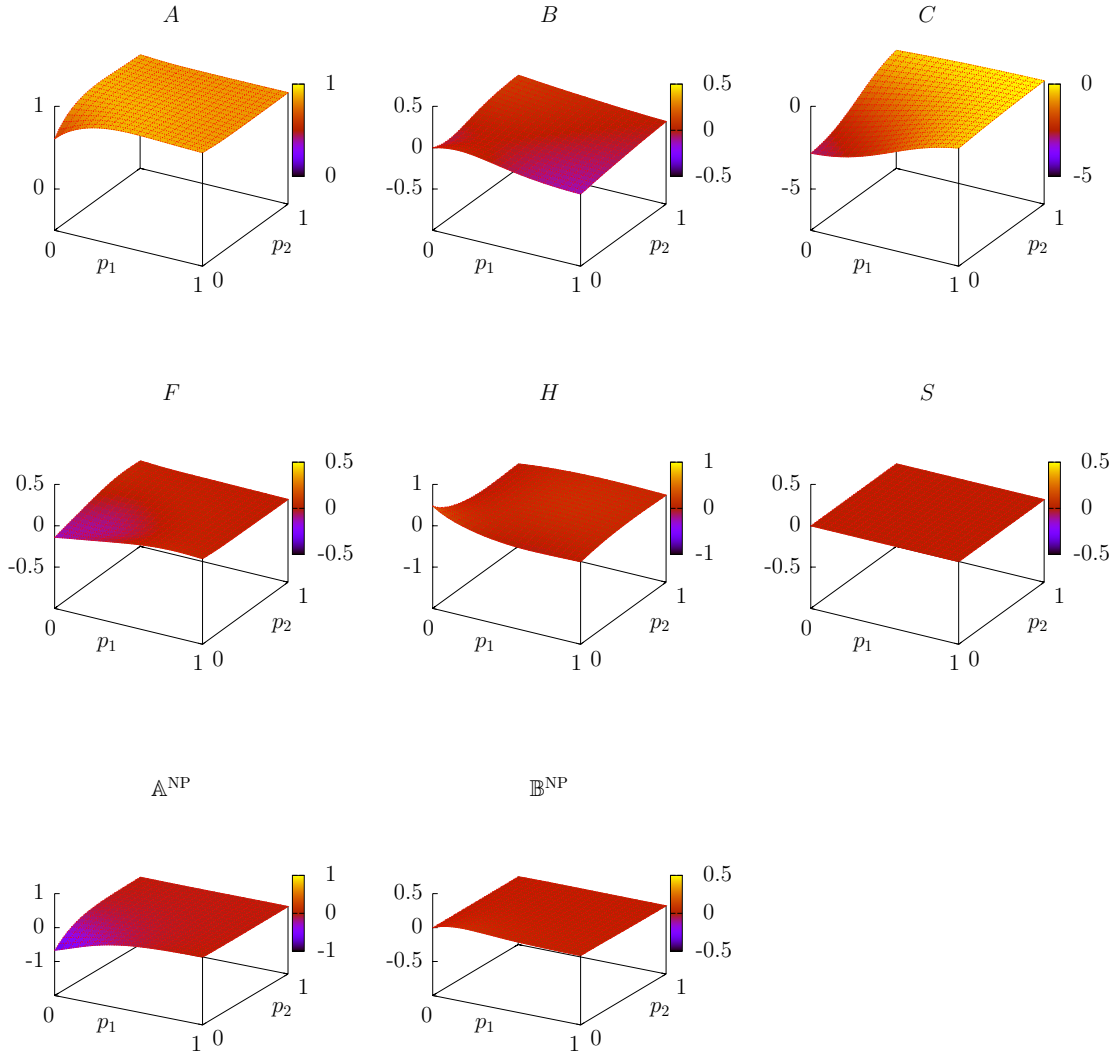


**Figure 10.**  $\xi = 1.0$ ,  $N_{\max}^{\text{P}} = 3$ ,  $N_{\max}^{\text{V}} = 3$ ,  $\cos\theta_{p_1,p_2} = 1/4$ .

## 6 Discussion

### 6.1 Comparison with other approaches

The majority of the literature on this subject is centered around 4D Yang-Mills theory; however, lattice studies (described shortly) have shown that Green's functions in 3D and 4D exhibit similar qualitative behavior. Nevertheless, we will try our best to directly compare our results with those obtained in 3D, to the extent that they exist.

The gluon propagator is an interesting quantity, despite not being directly related to any physical observable.  $G_T$  as depicted in Fig. 8 violates reflection positivity, that is, it does not have a Källén-Lehmann representation in terms of a positive spectral density. Hence, in (3+1) dimensions (or in our case (2+1) dimensions)  $G_T$  can not describe the

$a_0^{\{GT\}}$	-1.56e-01	$a_1^{\{GT\}}$	-1.03e+00	$a_2^{\{GT\}}$	-9.14e-01	$a_3^{\{GT\}}$	-4.47e-01	$b_1^{\{GT\}}$	4.11e+00	$b_2^{\{GT\}}$	4.10e+00
$b_3^{\{GT\}}$	3.82e+00	$a_2^{\{\Delta\}}$	1.79e-01	$a_3^{\{\Delta\}}$	1.13e-01	$b_1^{\{\Delta\}}$	1.73e+00	$b_2^{\{\Delta\}}$	3.49e+00	$b_3^{\{\Delta\}}$	1.75e+00
$a_{000}^{\{H\}}$	1.02e-01	$a_{100}^{\{H\}}$	-4.98e-02	$a_{110}^{\{H\}}$	-2.73e-01	$a_{111}^{\{H\}}$	-5.15e-01	$a_{200}^{\{H\}}$	-8.11e-01	$a_{210}^{\{H\}}$	1.40e-01
$a_{300}^{\{H\}}$	5.49e-01	$b_{100}^{\{H\}}$	1.19e+00	$b_{110}^{\{H\}}$	1.29e-01	$b_{111}^{\{H\}}$	2.38e-01	$b_{200}^{\{H\}}$	1.04e-01	$b_{210}^{\{H\}}$	-1.77e-01
$b_{300}^{\{H\}}$	3.20e-01	$a_{000}^{\{A\}}$	-2.77e-01	$a_{001}^{\{A\}}$	-7.66e-01	$a_{002}^{\{A\}}$	3.70e-01	$a_{003}^{\{A\}}$	8.59e-02	$a_{100}^{\{A\}}$	-9.45e-01
$a_{101}^{\{A\}}$	4.90e-01	$a_{102}^{\{A\}}$	-5.26e-02	$a_{110}^{\{A\}}$	7.11e-01	$a_{111}^{\{A\}}$	-8.68e-01	$a_{200}^{\{A\}}$	7.03e-02	$a_{201}^{\{A\}}$	-3.46e-01
$a_{210}^{\{A\}}$	-2.06e+00	$a_{300}^{\{A\}}$	-7.44e-02	$b_{001}^{\{A\}}$	1.54e+00	$b_{002}^{\{A\}}$	5.90e-01	$b_{003}^{\{A\}}$	6.73e-01	$b_{100}^{\{A\}}$	6.22e+00
$b_{101}^{\{A\}}$	8.78e-01	$b_{102}^{\{A\}}$	7.12e-01	$b_{110}^{\{A\}}$	1.85e+00	$b_{111}^{\{A\}}$	-6.23e-01	$b_{200}^{\{A\}}$	1.93e+00	$b_{201}^{\{A\}}$	-2.77e-01
$b_{210}^{\{A\}}$	-1.69e-01	$b_{300}^{\{A\}}$	3.42e-01	$a_{000}^{\{C\}}$	-1.53e+00	$a_{001}^{\{C\}}$	-1.74e+00	$a_{002}^{\{C\}}$	-6.63e-01	$a_{003}^{\{C\}}$	3.15e-02
$a_{100}^{\{C\}}$	5.94e-02	$a_{101}^{\{C\}}$	-2.47e-01	$a_{102}^{\{C\}}$	-2.09e-02	$a_{110}^{\{C\}}$	3.44e-01	$a_{111}^{\{C\}}$	-4.98e-01	$a_{200}^{\{C\}}$	-2.97e+00
$a_{201}^{\{C\}}$	6.72e-01	$a_{210}^{\{C\}}$	-4.27e-02	$a_{300}^{\{C\}}$	5.05e-01	$b_{001}^{\{C\}}$	4.11e-01	$b_{002}^{\{C\}}$	6.14e-01	$b_{003}^{\{C\}}$	7.04e-01
$b_{100}^{\{C\}}$	2.19e-01	$b_{101}^{\{C\}}$	5.53e-01	$b_{102}^{\{C\}}$	6.94e-01	$b_{110}^{\{C\}}$	4.13e-01	$b_{111}^{\{C\}}$	6.53e-01	$b_{200}^{\{C\}}$	3.68e-01
$b_{201}^{\{C\}}$	6.20e-01	$b_{210}^{\{C\}}$	5.21e-01	$b_{300}^{\{C\}}$	4.46e-01	$a_{000}^{\{F\}}$	-5.67e-02	$a_{001}^{\{F\}}$	-3.53e-03	$a_{002}^{\{F\}}$	9.77e-03
$a_{003}^{\{F\}}$	4.70e-01	$a_{100}^{\{F\}}$	-4.18e-02	$a_{101}^{\{F\}}$	-1.96e-02	$a_{102}^{\{F\}}$	3.20e-01	$a_{110}^{\{F\}}$	-5.84e-02	$a_{111}^{\{F\}}$	2.00e-01
$a_{200}^{\{F\}}$	-5.23e-02	$a_{201}^{\{F\}}$	2.57e-01	$a_{210}^{\{F\}}$	1.37e-01	$a_{300}^{\{F\}}$	2.28e-01	$b_{001}^{\{F\}}$	9.96e-01	$b_{002}^{\{F\}}$	9.96e-01
$b_{100}^{\{F\}}$	9.97e-01	$b_{101}^{\{F\}}$	9.96e-01	$b_{102}^{\{F\}}$	9.97e-01	$b_{110}^{\{F\}}$	9.98e-01	$b_{111}^{\{F\}}$	9.97e-01	$b_{200}^{\{F\}}$	9.98e-01
$b_{201}^{\{F\}}$	9.97e-01	$b_{210}^{\{F\}}$	9.98e-01	$b_{210}^{\{A\}}$	9.99e-01	$b_{300}^{\{A\}}$	9.99e-01	$a_{000}^{\{A\}}$	-8.12e-01	$a_{001}^{\{A\}}$	-1.02e-01
$a_{002}^{\{A\}}$	2.02e-01	$a_{003}^{\{A\}}$	2.12e-01	$a_{010}^{\{A\}}$	3.59e-01	$a_{011}^{\{A\}}$	-6.42e-01	$a_{012}^{\{A\}}$	-3.44e-01	$a_{020}^{\{A\}}$	-3.01e-01
$a_{021}^{\{A\}}$	-1.23e-01	$a_{030}^{\{A\}}$	2.68e-01	$a_{100}^{\{A\}}$	-1.23e-01	$a_{101}^{\{A\}}$	-9.41e-02	$a_{102}^{\{A\}}$	-1.16e-01	$a_{110}^{\{A\}}$	-4.18e-01
$a_{111}^{\{A\}}$	4.75e-01	$a_{120}^{\{A\}}$	2.53e-02	$a_{200}^{\{A\}}$	3.50e-02	$a_{201}^{\{A\}}$	4.01e-01	$a_{210}^{\{A\}}$	-2.83e-01	$a_{300}^{\{A\}}$	-1.65e-01
$b_{001}^{\{A\}}$	6.26e+00	$b_{002}^{\{A\}}$	2.89e+00	$b_{003}^{\{A\}}$	1.82e+00	$b_{010}^{\{A\}}$	6.31e+00	$b_{011}^{\{A\}}$	2.81e+00	$b_{012}^{\{A\}}$	1.71e+00
$b_{020}^{\{A\}}$	2.96e+00	$b_{021}^{\{A\}}$	1.64e+00	$b_{030}^{\{A\}}$	1.57e+00	$b_{100}^{\{A\}}$	5.13e+00	$b_{101}^{\{A\}}$	2.43e+00	$b_{102}^{\{A\}}$	1.55e+00
$b_{110}^{\{A\}}$	2.36e+00	$b_{111}^{\{A\}}$	1.44e+00	$b_{120}^{\{A\}}$	1.36e+00	$b_{200}^{\{A\}}$	2.30e+00	$b_{201}^{\{A\}}$	1.43e+00	$b_{210}^{\{A\}}$	1.31e+00
$b_{300}^{\{A\}}$	1.38e+00	$a_{000}^{\{B\}}$	1.43e-01	$a_{001}^{\{B\}}$	-3.00e-02	$a_{002}^{\{B\}}$	1.92e-01	$a_{010}^{\{B\}}$	1.06e-01	$a_{011}^{\{B\}}$	-1.90e-01
$a_{020}^{\{B\}}$	2.20e-01	$a_{100}^{\{B\}}$	2.53e-01	$a_{101}^{\{B\}}$	3.20e-01	$a_{110}^{\{B\}}$	-3.44e-02	$a_{200}^{\{B\}}$	-4.49e-01	$a_{00}^{\{B\}}$	2.52e-01
$a_{01}^{\{B\}}$	-5.05e-01	$a_{02}^{\{B\}}$	8.21e-02	$a_{10}^{\{B\}}$	-4.71e-02	$a_{11}^{\{B\}}$	2.61e-01	$a_{20}^{\{B\}}$	2.67e-01	$b_{001}^{\{B\}}$	1.00e+00
$b_{002}^{\{B\}}$	1.00e+00	$b_{003}^{\{B\}}$	1.00e+00	$b_{010}^{\{B\}}$	9.99e-01	$b_{011}^{\{B\}}$	1.00e+00	$b_{012}^{\{B\}}$	1.00e+00	$b_{020}^{\{B\}}$	1.00e+00
$b_{021}^{\{B\}}$	1.00e+00	$b_{030}^{\{B\}}$	1.00e+00	$b_{100}^{\{B\}}$	1.00e+00	$b_{101}^{\{B\}}$	1.00e+00	$b_{102}^{\{B\}}$	1.00e+00	$b_{110}^{\{B\}}$	1.00e+00
$b_{111}^{\{B\}}$	1.00e+00	$b_{120}^{\{B\}}$	1.00e+00	$b_{200}^{\{B\}}$	1.00e+00	$b_{201}^{\{B\}}$	1.00e+00	$b_{210}^{\{B\}}$	1.00e+00	$b_{300}^{\{B\}}$	1.01e+00

Table 2.  $\xi = 0.0$  variational coefficients

correlations of physical particles. This violation of reflection positivity is allowed despite its apparent contradiction with the Osterwalder-Schrader axioms; after all, we are dealing with a confining theory, so there is no one-to-one correspondence between fields and physical particles. This is further discussed in greater detail in [31], but the main point is that this behavior signals confinement.

The only propagating degrees of freedom that we can (in principle) observe are color singlet bound states, *glueballs* for instance. Hence, gluonic two and three point functions are not “physical,” and, in general the results we have presented are  $\xi$  dependent, which is not necessarily a bad thing. Indeed our intention is to use these results to compute gauge-invariant observables in some later publication.

However, in the mean time, we are stuck with analyzing  $\langle AA \rangle$  and  $\langle c\bar{c} \rangle$  as well as the vertices. Though arguably our best insight into IR QCD comes from the lattice, there have been many notable *first-principles* based speculations about the specific IR form of these functions. In general, the main point of contention is the exact value of  $G_T(0)$ . The most popular schools of thought can be summarized as follows...

### 6.1.1 The Gribov-Zwanziger Confinement Hypothesis

In his study on gauge-fixing and gauge copies in Yang-Mills theory [32], Gribov proposed that at one loop, the IR behavior of the gluon and ghost propagators is

$$G_T(p) \sim \frac{p^2}{p^4 + m^4}, \quad \Delta(p)|_{p^2 \rightarrow 0} \sim \frac{1}{p^4}. \quad (6.1)$$

This form has the generic feature that  $G_T$  vanishes at zero momentum, and moreover,  $\Delta$  experiences  $1/p^4$  IR enhancement, which can possibly be interpreted as signaling linear confinement (in 4D, or course). This form of  $G_T$  and  $\Delta$  was later advocated by Zwanziger, primarily because it vanishes at  $p = 0$ , which is in accordance with his theorem that  $G_T(0)$  (in Landau gauge) must vanish on any finitely spaced lattice in the infinite volume limit [33].

This proposal should be regarded as being fairly dated, and it is not in agreement with any of the more recent lattice data. It also does not accord with the behavior we determine by solving the 3PI problem.

### 6.1.2 Schwinger-Dyson Equations

These arguments [34] are based on obtaining solutions to a truncated set of Schwinger-Dyson equations for the gluon and ghost propagators, and in a sense, are very reminiscent of what we are doing here. If we assume power behavior of the gluon and ghost propagators in the infrared,

$$p^2 G_T(p) \sim (p^2)^{\kappa_G}, \quad p^2 \Delta(p) \sim (p^2)^{-\kappa_\Delta}, \quad (6.2)$$

then Ref. [35] claims that  $\kappa_G, \kappa_\Delta$  must satisfy

$$\kappa_G = 2\kappa_\Delta + (4 - D)/2, \quad (6.3)$$

and specifically in 3 dimensions  $\kappa_G = 0.2952$ , implying that the gauge field propagator goes to zero and the ghost propagator diverges more strongly than  $1/p^2$ . However this result assumes that the loop integral giving rise to a self-energy at momentum  $p$  is dominated by momenta of order  $p$ , whereas we find for small  $p$  that it is instead dominated by momenta of order  $g^2 N$ . Therefore it is not clear to us that this result of Ref. [35] is robust, see also [36]. It is also contradicted by more recent studies [37, 38], which give results (in 4 dimensions) showing  $G_T(p)$  going over to a constant, and  $\Delta(p) \propto p^{-2}$ , in the infrared. These studies are in at least qualitative agreement with lattice investigations. However, since in general Schwinger-Dyson based approaches are reliant on many simplifying approximations, they have yet to produce any quantitative agreement.

### 6.1.3 Observations From the Lattice

There is a wealth of lattice data related to this subject, and fortunately, different sources are generally in agreement. Simulations have been performed on very large lattices ( $V = 96^4$  [39, 40],  $V = 80^4$  [41],  $V = 128^4$  and  $V = 320^3$  [42–44]), from which one observes qualitative agreement between the results for 3D and 4D (hence we will intermittently compare 3D

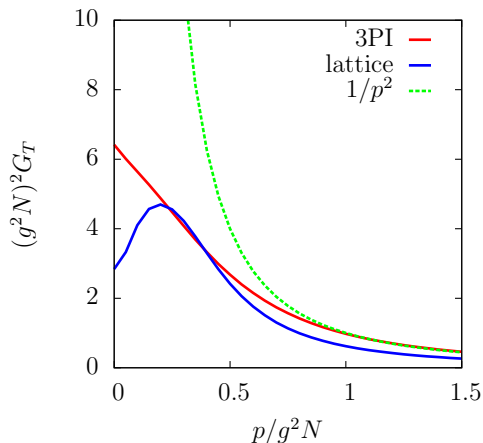


**Figure 11.** A comparison between the results of our calculation ( $G_T(p)$  in Landau gauge) and a reproduction of the plot of  $aD(p)$  (appropriately rescaled) in [44]. A free  $1/p^2$  propagator is shown for reference.

and 4D data, but *never* 2D). The generic finding is that  $p^2\Delta(p)|_{p^2\rightarrow 0}$  and  $G_T(0)$  are finite and nonzero.

However,  $G_T(0)$  is often seen to scale inversely with volume so it remains an open question as to whether the Zwanziger hypothesis is observable, and it is not known at what volume one should expect to see this effect. The results in Landau gauge currently depict a  $1/V^\alpha$  scaling for  $G_T$  but it is generally not observed that  $G_T(0) \rightarrow 0$  as  $V \rightarrow \infty$ .

All of the works cited above specifically employ the lattice implementation of Landau gauge. In fact, it is only fairly recently that preliminary 3D and 4D results in Feynman gauge have been made available [45].

In Fig. 11 our data is compared directly to the results in [42–44]. Their calculation was performed for SU(2) on an  $320^3$  3D lattice with  $\beta = 4/ag^2 = 3.0$ . To facilitate the comparison we have recast their results so momentum is scaled by  $g^2N$ . Their results are qualitatively similar to ours but differ quantitatively at the factor-of-2 level in the deep IR. This might indicate a limitation of the large- $N$  expansion, or it might simply indicate a failure of the 3PI method.

## 6.2 Slavnov-Taylor Identities

Planar diagrams on their own form a gauge invariant subset of the full loop expansion [46]. One may hope that in resumming a “dominant” or “important” set of planar diagrams (which is what hope to be doing here) gauge invariance is approximately conserved. This can be measured seeing to what extent our resulting two and three-point functions violate the Ward-Slavnov-Taylor (WST) identities. For the gluon propagator, we have

$$p^\mu p^\nu G_{\mu\nu} = \xi, \quad (6.4)$$

with deviations from this identity shown in Fig. 12.

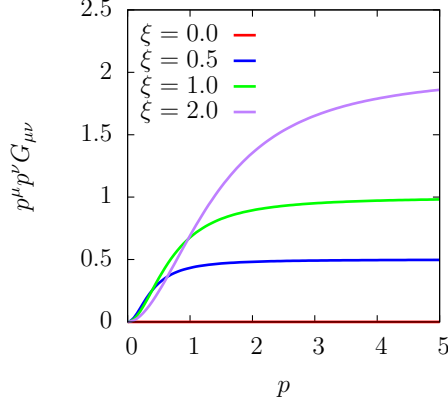


**Figure 12.** Propagator Ward Identity

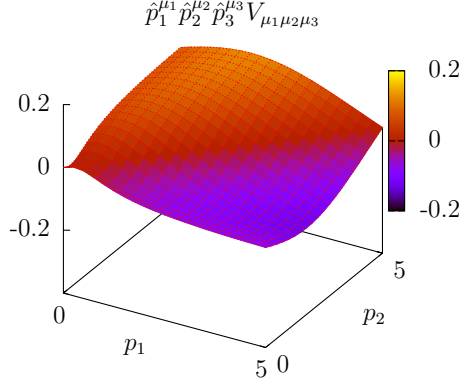


**Figure 13.** Vertex Ward Identity

In its most general form, the WST identity for the gluon three-vertex is

$$\begin{aligned}
 p_1^{\mu_1} V_{\mu_1 \mu_2 \mu_3}(p_1, p_2, p_3) &= \frac{F(p_1)}{J(p_3)} (p_3^2 g_{\alpha \mu_3} - p_{3\alpha} p_{3\mu_3}) \mathbb{V}_{\mu_2}^\alpha(p_3, p_1, p_2) \\
 &\quad - \frac{F(p_1)}{J(p_2)} (p_2^2 g_{\alpha \mu_2} - p_{2\alpha} p_{2\mu_2}) \mathbb{V}_{\mu_3}^\alpha(p_2, p_1, p_3), \quad (6.5)
 \end{aligned}$$

where  $F$  and  $J$  are defined in this context as  $J(p) = p^2 G_T(p)$  and  $F(p) = p^2 \Delta(p)$ .  $\mathbb{V}$  with two Lorentz indices is given by

$$\begin{aligned}
 \mathbb{V}_{\mu_3}^\alpha(p_1, p_2, p_3) &= g_{\mu_3}^\alpha a(p_3, p_2, p_1) - p_3^\alpha p_{2\mu_3} b(p_3, p_2, p_1) + p_1^\alpha p_{3\mu_3} c(p_3, p_2, p_1) \\
 &\quad + p_3^\alpha p_{1\mu_3} d(p_3, p_2, p_1) + p_1^\alpha p_{1\mu_3} e(p_3, p_2, p_1) \quad (6.6)
 \end{aligned}$$

which is related to the usual ghost-gluon vertex via  $\mathbb{V}_{\mu_3}(p_1, p_2, p_3) = p_{1\alpha} \mathbb{V}_{\mu_3}^\alpha(p_1, p_2, p_3)$

(following once again with the decomposition in [28]). From this identity one obtains

$$p_1^{\mu_1} p_2^{\mu_2} p_3^{\mu_3} V_{\mu_1 \mu_2 \mu_3}(p_1, p_2, p_3) = 0. \quad (6.7)$$

With  $\hat{p}^\mu \equiv p^\mu/p$ , the deviation from the vertex ward identity is show in Fig. 13 for Landau gauge. As previously, the vertex is a function of 3 variables, so to make a 2+1 dimensional plot we have fixed an angular variable to  $\cos \theta_{p_1 p_2} = 1/4$ .

## 7 Conclusions

We have successfully found the propagators and vertices which extremize the 3-loop, 3-particle-irreducibly action of QCD in 3 dimensions (the all-threes problem). We did so by writing a nonlinear variational *Ansatz* for three propagators (ghosts and the transverse and longitudinal components of gluons) and for eight vertices (two tensor structures for ghost-gluon vertices and six tensor structures for three-gluon vertices). To avoid divergences it was necessary to add and subtract terms to 1 and 2-loop self-energies; the added terms are computed in  $\overline{\text{MS}}$ , the subtraction renders the remaining numerical integrals finite. It was also necessary to compute the first loop corrections to 2-point and 3-point functions at large momentum explicitly and to incorporate these corrections into our *Ansätze* for those functions.

The most urgent task is to test the resulting resummation against exact nonperturbative results in 3D QCD by comparing the values of gauge invariant questions. For instance, one should be able to evaluate the  $\langle F^2(x) F^2(0) \rangle$  correlator, whose Fourier transform gives the lowest glueball mass. It might also be possible to evaluate the correlator of two field strengths connected by a Wilson line, which is of interest in evaluating the Debye screening mass in full QCD [47, 48]. Slightly extending our treatment to include a fundamental representation scalar, it should be possible to explore the 3D SU(2)+Higgs phase diagram, which can also be found nonperturbatively on the lattice [1].

Unfortunately it is not possible to compute the pressure of 3D Yang-Mills theory at the 3PI level, because the nontrivial contributions to the pressure arise at 4 loops. Evaluating the pressure would require a solution to the 4-loop 3PI or 4PI problem. Extending our approach to the 4-loop 4PI treatment would not raise any new conceptual issues, since all potential UV divergences in the extremization procedure are already encountered at the level of the 3-loop 3PI problem. It would be interesting to do so because the non-perturbative contribution to the pressure of 3D Yang-Mills theory is needed to compute the  $g^6$  term in the pressure for full QCD [17, 49]. However the extension to 4 loops and 4PI would be prohibitively difficult because the diagram generation and loop integration would become even more cumbersome and the number of possible tensor structures for the 4-point function is large.

Having studied the 3D theory, it appears to us that the extension to 4 or 3+1 dimensions will be extremely difficult. The problem is that one is simultaneously solving non-perturbative infrared physics and (perturbative) ultraviolet physics. The effective action is extremely sensitive to the ultraviolet form of the propagators and vertices; a procedure along the lines of what we have done here encounters quadratic UV divergences at every

loop order when evaluating self-energies, and quartic divergences when varying the propagators in a way which changes their UV behavior – at every loop order. It would be much harder to “cover up” gauge non-invariance in 4D because divergently large gauge boson masses would arise at every loop order, whereas we only encountered them at one loop (at two loops there were logs but they all cancel). Thus it is not clear what additional techniques would have to be developed to successfully extend our procedure to 4 dimensions. We will leave this for future investigation after we know whether the 3-loop treatment is successful in describing nonperturbative physics.

## Acknowledgments

We are grateful to Jürgen Berges and Mikko Laine for useful conversations. This work was supported in part by the Natural Sciences and Engineering Research Council of Canada.

## A Computations involving Bare Diagrams

Since we are working in three Euclidean dimensions, it is useful to now state the bare Feynman rules (with  $V_{\mu_1\mu_2\mu_3}^{(0)a_1a_2a_3} = F^{a_1a_2a_3}V_{\mu_1\mu_2\mu_3}^{(0)}$  and  $\mathbb{V}_{\mu_1\mu_2\mu_3}^{(0)a_1a_2a_3} = F^{a_1a_2a_3}\mathbb{V}_{\mu_1\mu_2\mu_3}^{(0)}$ )

$$gV_{\mu_1\mu_2\mu_3}^{(0)}(p_1, p_2, p_3) = g((p_2 - p_3)_{\mu_1}g_{\mu_2\mu_3} + (p_3 - p_1)_{\mu_2}g_{\mu_1\mu_3} + (p_1 - p_2)_{\mu_3}g_{\mu_1\mu_2}) \quad (\text{A.1})$$

$$g\mathbb{V}_{\mu_3}^{(0)}(p_1, p_2, p_3) = gp_{1\mu_3} \quad (\text{A.2})$$

$$\begin{aligned} g^2V_{\mu\nu\rho\tau}^{(0)abcd} = g^2 & \left( F^{abe}F^{cde}(g_{\mu\rho}g_{\nu\tau} - g_{\mu\tau}g_{\nu\rho}) \right. \\ & + F^{ace}F^{dbe}(g_{\mu\tau}g_{\nu\rho} - g_{\mu\nu}g_{\rho\tau}) \\ & \left. + F^{ade}F^{bce}(g_{\mu\nu}g_{\rho\tau} - g_{\mu\rho}g_{\nu\tau}) \right) \end{aligned} \quad (\text{A.3})$$

noting especially the overall sign of the four vertex.  $F^{abc}$  are the generators of the adjoint representation, defined in terms of the usual  $\text{SU}(N)$  structure factors by  $F^{abc} = -if^{abc}$ .  $F^{iab}F^{jba} = C_A\delta_{ij}$ , and for  $\text{SU}(N)$ ,  $C_A = N$ . The bare propagators are simply given by

$$G_{\mu\nu}^{(0)}(p) = \frac{1}{p^2}(\mathbf{T}_{\mu\nu} + \xi\mathbf{L}_{\mu\nu}) \quad (\text{A.4})$$

$$\Delta^{(0)}(p) = \frac{1}{p^2} \quad (\text{A.5})$$

with the transverse and longitudinal polarization tensors as defined earlier (color indices are suppressed). Finally the loop integral in  $D = 3 + 2\epsilon$  dimensions is defined as

$$\int_q \equiv \left( \frac{4\pi}{\mu^2 e^\gamma} \right)^\epsilon \int \frac{d^D q}{(2\pi)^D}. \quad (\text{A.6})$$

### A.1 Gluon Self-Energy

The gluon self-energy contains diagrams that superficially diverge linearly (one loop) and logarithmically (two loops); however, when computed in dimensional regularization, one finds that the sum of all one and two-loop contributions to the self-energy is UV finite.

At one loop, there are three diagrams, only two of which are nonzero in dimensional regularization.

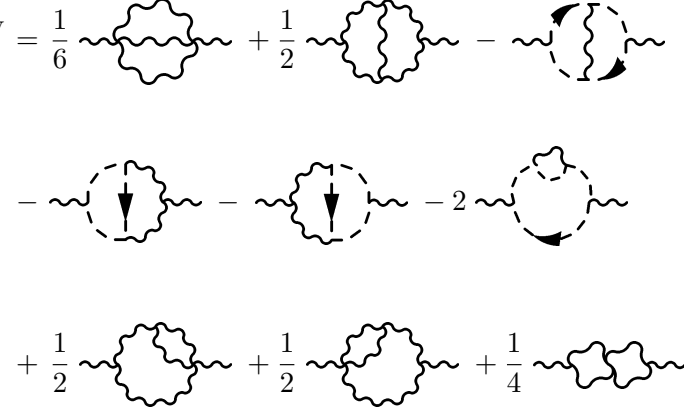
$$\Pi_{\mu\nu}^{\text{B}(1,\epsilon)} = \frac{1}{2} \text{diagram}_1 + \frac{1}{2} \text{diagram}_2 - \text{diagram}_3 \quad (\text{A.7})$$


Keeping terms up to  $\mathcal{O}(\epsilon)$  for convenience, the result is found to be

$$\Pi_{\mu\nu}^{\text{B}(1,\epsilon)} = \frac{g^2 N p^{1+2\epsilon}}{64 \mu^{2\epsilon}} [(\xi^2 + 2\xi + 11)(1 - 2\epsilon \log 2) + \epsilon(12 - 12\xi - 2\xi^2)] \mathbf{T}_{\mu\nu} \quad (\text{A.8})$$

$$= p \left( \frac{p^{2\epsilon}}{\mu^{2\epsilon}} \right) \Pi_{\mu\nu}^{\text{B}(1,\epsilon)} \mathbf{T}_{\mu\nu} \quad (\text{A.9})$$

UV divergences only start to arise at the two-loop level, and on a diagram by diagram basis, these are all proportional to  $g_{\mu\nu}$ . The two-loop self-energy also contains diagrams that are potentially IR divergent, and these will be handled separately. Defining

$$\begin{aligned} \Pi_{\mu\nu}^{\text{B}(2,\epsilon)\text{UV}} = & \frac{1}{6} \text{diagram}_1 + \frac{1}{2} \text{diagram}_2 - \text{diagram}_3 \\ & - \text{diagram}_4 - \text{diagram}_5 - 2 \text{diagram}_6 \\ & + \frac{1}{2} \text{diagram}_7 + \frac{1}{2} \text{diagram}_8 + \frac{1}{4} \text{diagram}_9 \end{aligned} \quad (\text{A.10})$$


where it should be noted that the “figure eight” diagram (proportional to 1/4) is strictly finite, but is included for completeness. An actual computation yields

$$\begin{aligned} \Pi_{\mu\nu}^{\text{B}(2,\epsilon)\text{UV}} = & \frac{g^4 N^2 p^{4\epsilon}}{\pi^2 \mu^{4\epsilon}} \left[ \frac{(\xi + 2)(\xi^2 + 2\xi + 1)}{768\epsilon} g_{\mu\nu} \right. \\ & + \frac{8(7\xi^3 + 75\xi^2 + 221\xi + 233) - 18\zeta(2)(\xi^2 + 3)(\xi^2 + 2\xi^2 + 17)}{12288} \mathbf{T}_{\mu\nu} \\ & \left. - \frac{7\xi^3 + 32\xi^2 + 79\xi + 42}{768} \mathbf{L}_{\mu\nu} \right]. \end{aligned} \quad (\text{A.11})$$

The IR regulation is achieved via the introduction of a fictitious mass  $m^2$  in the denominators of both of the divergent diagrams. In  $D = 3 + 2\epsilon$ , the IR regulated integrals have

the following form

$$\text{Diagram (A.12)} = g^2 \int_q V_{\mu\nu\alpha\beta}^{(0)} \frac{\Pi^{\text{B}(1,\epsilon)} g^{\alpha\beta} - \frac{q^\alpha q^\beta}{q^2+m^2}}{\mu^{2\epsilon}} \frac{1}{(q^2+m^2)^{\frac{3}{2}-\epsilon}} \quad (\text{A.12})$$

$$\text{Diagram (A.13)} = g^2 \int_q V_{\mu\alpha\delta}^{(0)} V_{\nu\beta\kappa}^{(0)} \frac{\Pi^{\text{B}(1,\epsilon)} g^{\alpha\beta} - \frac{q^\alpha q^\beta}{q^2+m^2}}{\mu^{2\epsilon}} \frac{g^{\delta\kappa} - (1-\xi) \frac{(p+q)^\delta (p+q)^\kappa}{(p+q)^2}}{(q^2+m^2)^{\frac{3}{2}-\epsilon}} \frac{1}{(p+q)^2}. \quad (\text{A.13})$$

Including the IR regulator  $m^2$  in exactly this manner was found to yield *relatively* simple and compact final expressions. Adding together these two diagrams,

$$\Pi_{\mu\nu}^{\text{B}(2,\epsilon)\text{IR Reg}} = \text{Diagram (A.14)} + \frac{1}{2} \text{Diagram (A.14)} \quad (\text{A.14})$$

we obtain

$$\begin{aligned} \Pi_{\mu\nu}^{\text{B}(2,\epsilon)\text{IR Reg}} &= \frac{g^4 N^2 p^{4\epsilon}}{\pi^2 \mu^{4\epsilon}} \left[ -\frac{(\xi+2)(\xi^2+2\xi+1)}{768\epsilon} g_{\mu\nu} \right. \\ &+ \frac{1}{2304} \left( 3(\xi+2)(\xi^2+2\xi+11) \log \frac{16p^4}{m^4} + \frac{m^4}{p^4} (9\xi^3+15\xi^2+93\xi-33) \right. \\ &+ \frac{m^2}{p^2} (-6\xi^3+48\xi^2+54\xi+660) + (15\xi^3+148\xi^2+299\xi+830) \\ &- 3(\xi^2+2\xi+11) \left[ \frac{(3\xi-1)m^6 + (11-3\xi)(m^4 p^2 + m^2 p^4) + (2\xi-2)p^6}{p^4(p^2+m^2)} \right. \\ &+ \left. \left. \frac{\tanh^{-1} \sqrt{\frac{p^2}{p^2+m^2}}}{p^3(p^2+m^2)^{3/2}} \left( (4\xi+8)m^6 + (9\xi+43)p^2 m^4 + (4\xi+34)p^4 m^2 \right) \right] \right) \mathbf{T}_{\mu\nu} \\ &+ \frac{1}{2304} \left( 3(\xi+2)(\xi^2+2\xi+11) \log \frac{16p^4}{m^4} - \frac{m^2}{p^2} (24\xi^3+96\xi^2+360\xi+528) \right. \\ &+ (21\xi^3+100\xi^2+245\xi+170) \\ &+ 6(\xi^2+2\xi+11) \frac{\tanh^{-1} \sqrt{\frac{p^2}{p^2+m^2}}}{p^3(p^2+m^2)^{1/2}} \left( (4\xi+8)m^4 \right. \\ &\left. \left. - (\xi-1)m^2 p^2 - (2\xi+4)p^4 \right) \right) \mathbf{L}_{\mu\nu} \left. \right]. \quad (\text{A.15}) \end{aligned}$$

As expected all of the UV divergences cancel between diagrams, and hence we can safely take the  $\epsilon \rightarrow 0$  limit and be left with something finite,

$$\lim_{\epsilon \rightarrow 0} \left( \Pi_{\mu\nu}^{\text{B}(2,\epsilon)\text{UV}} + \Pi_{\mu\nu}^{\text{B}(2,\epsilon)\text{IR Reg}} \right) \neq \pm\infty. \quad (\text{A.16})$$



of Appel's hypergeometric function [50]

$$F_4(a, b; c, d|x, y) = \sum_{i=0}^{\infty} \sum_{j=0}^{\infty} \frac{(a)_{i+j}(b)_{i+j}}{(c)_i(d)_j} \frac{x^i y^j}{i! j!} \quad (\text{A.25})$$

making use of the Pockhammer symbol  $(a)_i = \Gamma(a+i)/\Gamma(a)$ . In any (Euclidean) dimension, omitting the  $\overline{\text{MS}}$  scale, the expression reads

$$\begin{aligned} C_{\alpha\beta\gamma}^0 = & \frac{1}{(4\pi)^{D/2}\Gamma(\gamma)\Gamma(\beta)\Gamma(\alpha)\Gamma(D-\gamma-\beta-\alpha)} \left[ \right. \\ & (p_3^2)^{D/2-\gamma-\beta-\alpha}\Gamma(\gamma)\Gamma(\gamma+\beta+\alpha-D/2)\Gamma(D/2-\gamma-\beta)\Gamma(D/2-\gamma-\alpha) \\ & \times F_4\left(\gamma, \gamma+\beta+\alpha-D/2; \gamma+\beta-D/2+1, \gamma+\alpha-D/2+1 \middle| \frac{p_1^2}{p_3^2}, \frac{p_2^2}{p_3^2}\right) \\ & + (p_2^2)^{D/2-\gamma-\alpha}(p_3^2)^{-\beta}\Gamma(\beta)\Gamma(D/2-\alpha)\Gamma(D/2-\gamma-\beta)\Gamma(\gamma+\alpha-D/2) \\ & \times F_4\left(\beta, D/2-\alpha; \gamma+\beta-D/2+1, D/2-\gamma-\alpha+1 \middle| \frac{p_1^2}{p_3^2}, \frac{p_2^2}{p_3^2}\right) \\ & + (p_1^2)^{D/2-\gamma-\beta}(p_3^2)^{-\alpha}\Gamma(\alpha)\Gamma(D/2-\beta)\Gamma(D/2-\gamma-\alpha)\Gamma(\gamma+\beta-D/2) \\ & \times F_4\left(\alpha, D/2-\beta; D/2-\gamma-\beta+1, \gamma+\alpha-D/2+1 \middle| \frac{p_1^2}{p_3^2}, \frac{p_2^2}{p_3^2}\right) \\ & + \Gamma(D-\gamma-\beta-\alpha)(p_1^2)^{D/2-\gamma-\beta}(p_2^2)^{D/2-\gamma-\alpha}(p_3^2)^{\gamma-D/2} \\ & \times \Gamma(D/2-\gamma)\Gamma(\gamma+\beta-D/2)\Gamma(\gamma+\alpha-D/2) \\ & \left. \times F_4\left(D-\gamma-\beta-\alpha, D/2-\gamma; D/2-\gamma-\beta+1, D/2-\gamma-\alpha+1 \middle| \frac{p_1^2}{p_3^2}, \frac{p_2^2}{p_3^2}\right) \right]. \quad (\text{A.26}) \end{aligned}$$

At the one-loop level, the three-gluon and ghost-gluon vertices have the following form

$$\begin{aligned} gV_{\mu_1\mu_2\mu_3}^{(1)a_1a_2a_3}(p_1, p_2, p_3) = & gF^{a_1a_2a_3} \left[ A^{(1)}(p_1, p_2; p_3)\mathbf{A}_{\mu_1\mu_2\mu_3} + B^{(1)}(p_1, p_2; p_3)\mathbf{B}_{\mu_1\mu_2\mu_3} \right. \\ & + C^{(1)}(p_1, p_2; p_3)\mathbf{C}_{\mu_1\mu_2\mu_3} + F^{(1)}(p_1, p_2; p_3)\mathbf{F}_{\mu_1\mu_2\mu_3} \\ & + H^{(1)}(p_1, p_2, p_3)\mathbf{H}_{\mu_1\mu_2\mu_3} + S^{(1)}(p_1, p_2, p_3)\mathbf{S}_{\mu_1\mu_2\mu_3} \\ & \left. + \text{cyclic perms.} \right] \quad (\text{A.27}) \end{aligned}$$

$$gV_{\mu_3}^{(1)a_1a_2a_3}(p_1, p_2, p_3) = gF^{a_1a_2a_3} \left[ \mathbb{A}^{(1)}(p_1, p_2, p_3)p_{1\mu_3} + \mathbb{B}^{(1)}(p_1, p_2, p_3)p_{2\mu_3} \right] \quad (\text{A.28})$$

with the tensors  $\mathbf{A}$  through  $\mathbf{S}$  as defined in Section 4. The vertex functions are as follows:

$$\begin{aligned} A^{(1)}(p_1, p_2; p_3) = & -\frac{g^2 N}{1024p_1^3p_2^3p_3(p_1+p_2+p_3)^2} \left[ 16p_1^2p_2^2(p_1+p_2+p_3) \left[ 4(p_1-p_2)^2(p_1+p_2) \right. \right. \\ & + (5p_1^2+6p_1p_2+5p_2^2)p_3 + 3(p_1+p_2)p_3^2 + 6p_3^3] - 4[(p_1^2-p_2^2)^2(p_1^4+2p_1^3p_2 \\ & + 4p_1^2p_2^2+2p_1p_2^3+p_2^4) - 2p_1p_2(p_1+p_2)(p_1^4-4p_1^3p_2-2p_1^2p_2^2-4p_1p_2^3+p_2^4)p_3 \\ & - (p_1^6-11p_1^4p_2^2-16p_1^3p_2^3-11p_1^2p_2^4+p_2^6)p_3^2 + 8p_1^2p_2^2(p_1+p_2)p_3^3 \\ & - (p_1-p_2)^2(p_1^2+4p_1p_2+p_2^2)p_3^4 + 2p_1p_2(p_1+p_2)p_3^5 + (p_1^2+p_2^2)p_3^6] (1-\xi) \\ & + (p_1+p_2+p_3)^2 \left[ (p_1-p_2)^2(p_1^4+2p_1^3p_2+2p_1p_2^3+p_2^4) - 2(p_1+p_2)^3(p_1^2-3p_1p_2+p_2^2)p_3 \right. \\ & \left. \left. + 2(p_1^4-p_1^2p_2^2+p_2^4)p_3^2 - 2(p_1^3+p_2^3)p_3^3 + (p_1^2+p_2^2)p_3^4 \right] (1-\xi)^2 \right] \quad (\text{A.29}) \end{aligned}$$

$$\begin{aligned}
B^{(1)}(p_1, p_2; p_3) = & -\frac{g^2 N(p_1 - p_2)}{1024p_1^3 p_2^3 p_3^3 (p_1 + p_2 + p_3)^2} \left[ 16p_1^2 p_2^2 p_3^2 [2(p_1 + p_2)^3 \right. \\
& - 9(p_1 + p_2)^2 p_3 - 20(p_1 + p_2)p_3^2 - 9p_3^3] - 4[2p_1^2(p_1 - p_2)^2 p_2^2(p_1 + p_2)^3 \\
& + 4p_1^2 p_2^2 (p_1^2 - p_2^2)^2 p_3 - (p_1 + p_2)(p_1^6 + 2p_1^5 p_2 - 3p_1^4 p_2^2 - 4p_1^3 p_2^3 - 3p_1^2 p_2^4 + 2p_1 p_2^5 + p_2^6) p_3^2 \\
& + 2p_1 p_2 (p_1 + p_2)^2 (p_1^2 - 6p_1 p_2 + p_2^2) p_3^3 + (p_1 + p_2)(p_1^4 - 26p_1^2 p_2^2 + p_2^4) p_3^4 - 12p_1^2 p_2^2 p_3^5 \\
& + (p_1 + p_2)^3 p_3^6 - 2p_1 p_2 p_3^7 - (p_1 + p_2) p_3^8] (\xi - 1) \\
& + (p_1 + p_2 + p_3)^2 [2p_1^2(p_1 - p_2)^2 p_2^2(p_1 + p_2) - (p_1 + p_2)(p_1^4 + p_2^4) p_3^2 \\
& + 2(p_1 - p_2)^2 (p_1^2 + 3p_1 p_2 + p_2^2) p_3^3 - 2(p_1 + p_2)(p_1^2 + p_2^2) p_3^4 \\
& \left. + 2(p_1^2 + p_1 p_2 + p_2^2) p_3^5 - (p_1 + p_2) p_3^6] (1 - \xi)^2 \right] \tag{A.30}
\end{aligned}$$

$$\begin{aligned}
C^{(1)}(p_1, p_2; p_3) = & \frac{g^2 N}{512p_1^3 p_2^3 (p_1 + p_2) p_3 (p_1 + p_2 + p_3)^2} \left[ 48p_1^2 p_2^2 (p_1 + p_2)^2 p_3 \right. \\
& + [(p_1 - p_2)^2 (p_1 + p_2)^5 - 2p_1^3 p_2 (p_1 + p_2)^2 p_3 - 2p_1 p_2^3 (p_1 + p_2)^2 p_3 - p_1^4 (p_1 + p_2) p_3^2 \\
& - (p_1 + p_2) p_2^4 p_3^2 - (p_1 + p_2)^3 p_3^4 + 2p_1 p_2 p_3^5 + (p_1 + p_2) p_3^6] (\xi - 1)(3 + \xi) \\
& \left. + 2p_1^2 (p_1 + p_2) p_2^2 p_3^2 (81 + 5[2 + \xi]\xi) + 4p_1^2 p_2^2 p_3^3 (29 + [6 + \xi]\xi) \right] \tag{A.31}
\end{aligned}$$

$$\begin{aligned}
F^{(1)}(p_1, p_2; p_3) = & -\frac{g^2 N}{512p_1^3 p_2^3 (p_1 + p_2) p_3^3 (p_1 + p_2 + p_3)^3} \left[ [ - (p_1 - p_2)^2 (p_1 + p_2)^6 \right. \\
& - 3(p_1 - p_2)^2 (p_1 + p_2)^5 p_3] (\xi - 1)^2 (3 + \xi) + [(p_1 + p_2) p_3^7 (-3 + \xi)(3 + \xi) \\
& + (3 + \xi)(-20p_1^3 p_2 (p_1 + p_2)^2 p_3^2 - 20p_1 p_2^3 (p_1 + p_2)^2 p_3^2 - p_1^4 (p_1 + p_2) p_3^3 (9 + \xi) \\
& - p_2^4 (p_1 + p_2) p_3^3 (9 + \xi) + p_1^4 p_3^4 (11 + \xi) + 4p_1^3 p_2 p_3^4 (11 + \xi) + 4p_1 p_2^3 p_3^4 (11 + \xi) \\
& + p_2^4 p_3^4 (11 + \xi) - p_1^4 (p_1 + p_2)^2 p_3^2 (7 + 3\xi) - p_2^4 (p_1 + p_2)^2 p_3^2 (7 + 3\xi)] (\xi - 1) \\
& + 2p_1^2 p_2^2 (p_1 + p_2)^2 p_3^2 (-113 + 3\xi(-1 + [-5 + \xi]\xi)) \\
& + 2p_1^2 p_2^2 (p_1 + p_2) p_3^3 (-303 + \xi(-25 + [23 + \xi]\xi)) \\
& + 2p_1^2 p_2^2 p_3^4 (-215 + \xi(33 + [35 + 3\xi]\xi)) + [3(p_1 + p_2)^3 p_3^5 (\xi - 1) \\
& + 12(p_1 + p_2)(p_1^2 + p_2^2) p_3^5 - p_3^6 [5p_1^2 + 14p_1 p_2 + 5p_2^2 \\
& \left. - 3(p_1 + p_2)^2 \xi] (1 - \xi)(-3 - \xi) \right] \tag{A.32}
\end{aligned}$$

$$\begin{aligned}
H^{(1)}(p_1, p_2, p_3) = & \frac{g^2 N}{1024 p_1^3 p_2^3 p_3^3 (p_1 + p_2 + p_3)^3} \left[ \left[ p_1^9 + 6 [p_1^7 p_2 p_3 - p_1^5 p_2^3 p_3 - p_1^3 p_2^5 p_3 - p_1^5 p_2 p_3^3 \right. \right. \\
& - p_1^3 p_2 p_3^5] + 3 p_1^8 (p_2 + p_3) + 3 p_1 p_2^4 (p_2 - p_3)^2 (p_2 + p_3)^2 + 6 p_1 p_2^3 (p_2 - p_3)^2 p_3 (p_2 + p_3)^2 \\
& + 6 p_1 p_2 (p_2 - p_3)^2 p_3^3 (p_2 + p_3)^2 + 3 p_1 (p_2 - p_3)^2 p_3^4 (p_2 + p_3)^2 + p_2^4 (p_2 - p_3)^2 (p_2 + p_3)^3 \\
& + 2 p_2^3 (p_2 - p_3)^2 p_3 (p_2 + p_3)^3 + 2 p_2 (p_2 - p_3)^2 p_3^3 (p_2 + p_3)^3 \\
& + (p_2 - p_3)^2 p_3^4 (p_2 + p_3)^3 \Big] (\xi - 1)^2 (3 + \xi) + \left[ \left[ 2 p_1^2 p_2^5 p_3 (p_2 + p_3) \right. \right. \\
& + 2 p_1^2 p_2 p_3^5 (p_2 + p_3) \Big] (13 - \xi) + 2 \left[ p_1^3 p_2^6 + p_1^3 p_3^6 + p_1^6 p_2^2 (p_2 + p_3) + p_1^6 p_3^2 (p_2 + p_3) \right] (7 - \xi) \\
& + \left[ 2 p_1^7 p_2^2 - 4 p_1^5 p_2^4 + 2 p_1^7 p_3^2 - 4 p_1^5 p_3^4 - 4 p_1^4 p_2^4 (p_2 + p_3) + 2 p_1^2 p_2^6 (p_2 + p_3) \right. \\
& - 4 p_1^4 p_3^4 (p_2 + p_3) + 2 p_1^2 p_3^6 (p_2 + p_3) + 6 p_1 p_2^2 (p_2 - p_3)^2 p_3^2 (p_2 + p_3)^2 \\
& + 2 p_2^2 (p_2 - p_3)^2 p_3^2 (p_2 + p_3)^3 \Big] (5 + \xi) + 2 p_1^6 p_2 p_3 (p_2 + p_3) (11 + \xi) \\
& - \left. \left. \left[ 2 p_1^4 p_2^3 p_3 (p_2 + p_3) + 2 p_1^4 p_2 p_3^3 (p_2 + p_3) \right] (23 + \xi) \right] (\xi - 1) (3 + \xi) \right. \\
& + 4 p_1^4 p_2^2 p_3^2 (p_2 + p_3) (78 - 5\xi + 7\xi^3) - 2 \left[ p_1^3 p_2^4 p_3^2 + p_1^3 p_2^2 p_3^4 \right] (-225 + \xi(53 + [25 - 13\xi]\xi)) \\
& - 4 p_1^3 p_2^3 p_3^3 (-217 + 3\xi(17 + [7 - 5\xi]\xi)) + 4 p_1^5 p_2^2 p_3^2 (-18 + \xi(13 + [20 + \xi]\xi)) \\
& + \left. \left. \left[ 2 p_1^2 p_2^4 p_3^2 (p_2 + p_3) + 2 p_1^2 p_2^2 p_3^4 (p_2 + p_3) \right] (3 + \xi(-3 + [29 + 3\xi]\xi)) \right. \right. \\
& \left. \left. + 4 p_1^2 p_2^3 p_3^3 (p_2 + p_3) (111 + \xi(-25 + [-27 + 5\xi]\xi)) \right] \right. \tag{A.33}
\end{aligned}$$

$$S^{(1)}(p_1, p_2, p_3) = 0 \tag{A.34}$$

and, for instance, the regulator  $\omega^{(1)}$  mentioned in Section 4 is included in the  $A$  function by making the transformation

$$\frac{1}{p_1^3 p_2^3 p_3^3 (p_1 + p_2 + p_3)^2} \rightarrow \frac{1}{(p_1 + \omega^{(1)})^3 (p_2 + \omega^{(1)})^3 (p_3 + \omega^{(1)}) (p_1 + p_2 + p_3 + \omega^{(1)})^2} \tag{A.35}$$

and likewise for  $B$  through  $H$ . The one-loop ghost vertices are

$$\begin{aligned}
\mathbb{A}^{(1)}(p_1, p_2, p_3) = & \frac{g^2 N}{512 p_1 p_2 p_3^3 (p_1 + p_2 + p_3)} \left[ 16 p_3^2 \left[ -p_1^3 + p_1^2 (-p_2 + p_3) \right. \right. \\
& - (p_2 - p_3)^2 (p_2 + p_3) + p_1 (3 p_2^2 + 2 p_2 p_3 + p_3^2) \Big] + 4 (p_1 - p_2 - p_3) \left[ (p_1^2 - p_2^2)^2 \right. \\
& + 2 p_1 (p_1 - p_2) (p_1 + p_2) p_3 + (5 p_1 - p_2) (p_1 + p_2) p_3^2 + 2 (p_1 + p_2) p_3^3 - 2 p_3^4 \Big] (1 - \xi) \\
& - (p_1^2 - p_2^2 - p_3^2) \left[ (p_1 - p_2)^2 (p_1 + p_2) + (p_1 - p_2)^2 p_3 \right. \\
& \left. \left. + (p_1 + p_2) p_3^2 - 3 p_3^3 \right] (1 - \xi)^2 \right], \tag{A.36}
\end{aligned}$$

$$\begin{aligned}
\mathbb{B}^{(1)}(p_1, p_2, p_3) = & - \frac{g^2 N}{512 p_1 p_2 p_3^3 (p_1 + p_2 + p_3)} \left[ 32 p_1 p_3^2 \left[ (p_1 - p_2) p_2 + p_3^2 \right] \right. \\
& - 4 (p_1^2 - p_2^2 + p_3^2) \left[ p_1^3 + (p_2 - p_3) \left[ (p_2 + p_3)^2 - p_1 (p_2 + 3 p_3) - p_1^2 \right] \right] (1 - \xi) \\
& + (p_1^2 - p_2^2 + p_3^2) \left[ (p_1 - p_2)^2 (p_1 + p_2) + (p_1 - p_2)^2 p_3 \right. \\
& \left. \left. + (p_1 + p_2) p_3^2 - 3 p_3^3 \right] (1 - \xi)^2 \right]. \tag{A.37}
\end{aligned}$$

## B Phase space integrations

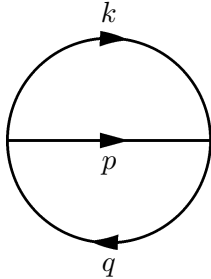
In performing numerical integrals over vacuum diagrams encountered in this paper we need efficient parametrizations of the phase space integrals. At two loops the most interesting diagram is the Setting Sun, at three loops it is the Mercedes diagram. All other diagrams can be solved by being reduced to these two (as we will describe), so we will concentrate on them.

In  $D$  dimensions an  $n$ -loop diagram involves  $nD$  real integrations. However the symmetry group  $O(D)$  helps reduce this because certain angular integrations are trivial. Namely, there are  $D(D-1)/2$  global angular integrations. Selecting  $n$   $D$ -vectors reduces  $O(D)$  to  $O(D-n)$  (for  $n \leq D-2$ ) or reduces it completely (for  $n \geq D-1$ ). Therefore, for  $n \leq D-2$ ,  $D(D-1)/2 - (D-n)(D-n-1)/2 = nD - n(n+1)/2$  of the integrals are global angular integrals which can be performed immediately since none of the invariants depend on them. This leaves  $n(n-1)/2$  nontrivial integrations, for  $n \leq D-2$ . For  $n \geq D-1$  there are  $nD - D(D-1)/2$  nontrivial integrations.

In an  $n$ -loop connected vacuum diagram built entirely with 3-point vertices there are  $3n-3$  propagators. For  $D=3$  and  $n \geq 2$  this happens to equal the number of integration variables. Therefore, in  $D=3$  dimensions, in diagrams composed using 3-point vertices and where each propagator has a distinct momentum (which is the case for 2PI or 3PI diagrams), it should be possible to arrange for the integration variables to be precisely the magnitudes of the momenta on all propagators. This is a very convenient choice, provided that all dot products of propagator momenta have simple enough expressions.

### B.1 Two loops: Setting Sun

We apply these ideas first to the Setting Sun diagram, that is, two vertices connected by three lines:



The “natural” integration variables are

$$\int \frac{d^3 p d^3 k}{(2\pi)^6} = \frac{8\pi^2}{(2\pi)^6} \int_0^\infty p^2 dp \int_0^\infty k^2 dk \int_{-1}^1 d \cos \theta_{pk} \quad (\text{B.1})$$

where we have performed the trivial integral over the Eulerian angles, in the form of the direction of the  $\vec{p}$  integral and the azimuthal angle of  $\vec{k}$  if  $\vec{p}$  is taken as the  $\vec{z}$  axis.

The dot product  $\vec{p} \cdot \vec{k} = pk \cos \theta_{pk}$  and

$$q^2 = (\vec{p} + \vec{k})^2 = p^2 + k^2 + 2pk \cos \theta_{pk} \quad \Rightarrow \quad \cos \theta_{pk} = \frac{q^2 - p^2 - k^2}{2pk}. \quad (\text{B.2})$$

If we change variables from  $p, k, \cos \theta_{pk}$  to  $p, k, q$  we should differentiate the above holding  $p, k$  fixed, giving

$$d \cos \theta_{pk} = \frac{q}{pk} dq. \quad (\text{B.3})$$

Therefore we can rewrite the integration as

$$\int \frac{d^3 p d^3 k}{(2\pi)^6} = \frac{1}{2^3 \pi^4} \int_0^\infty p dp \int_0^\infty k dk \int_{|p-k|}^{p+k} q dq = \frac{1}{2^6 \pi^4} \int_0^\infty dp^2 \int_0^\infty dk^2 \int_{(p-k)^2}^{(p+k)^2} dq^2 \quad (\text{B.4})$$

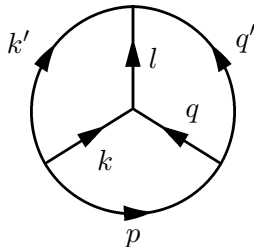
which are a convenient set of integration variables. In particular, all dot products we will encounter can be written directly in terms of the integration variables using

$$-\vec{p} \cdot \vec{q} = \frac{k^2 - p^2 - q^2}{2}, \quad -\vec{k} \cdot \vec{q} = \frac{p^2 - k^2 - q^2}{2}, \quad \vec{p} \cdot \vec{k} = \frac{q^2 - p^2 - k^2}{2}. \quad (\text{B.5})$$

The remaining two-loop diagram, the Figure-8, can be performed using the same integration variables; the two lines have momentum  $\vec{p}$  and  $\vec{k}$ , so the  $q$  integral can be done directly,  $\int q dq = 2pk$ . This sort of reduction always works, because we can always consider a 4-point vertex to be two three-point vertices connected by a propagator, with the propagator collapsed to a point. So diagrams containing 4-point vertices can be written with the same variables as the diagram containing this ‘‘collapsed’’ propagator.

## B.2 Three loops: Mercedes

Now we seek a similar set of integration variables for the Mercedes diagram,



Note that  $\vec{l} = \vec{k} + \vec{q}$  and similarly  $\vec{k}' = -\vec{p} - \vec{k}$  and  $\vec{q}' = \vec{p} - \vec{q}$ . The phase space is determined by the triple integral

$$\int \frac{d^3 p d^3 k d^3 q}{(2\pi)^9} = \int_0^\infty p^2 dp \int_0^\infty k^2 dk \int_0^\infty q^2 dq \frac{16\pi^2}{(2\pi)^9} \int_{-1}^1 d \cos \theta_{pk} \int_{-1}^1 d \cos \theta_{pq} \int_0^\pi d \phi_{pk;pq} \quad (\text{B.6})$$

where  $\phi$  is the azimuthal angle between the  $pk$  plane and the  $pq$  plane, we have used the symmetry of the  $\phi$  integration to reduce it from  $[0, 2\pi]$  to  $[0, \pi]$ , and Eulerian angles have again been performed.

Using the same trick as before, we can rewrite this integral as

$$\frac{1}{2^5 \pi^7} \int_0^\infty dp \int_0^\infty k dk \int_0^\infty q dq \int_{|p-k|}^{p+k} k' dk' \int_{|p-q|}^{p+q} q' dq' \int_0^\pi d \phi_{pq;pk}. \quad (\text{B.7})$$

and we would like to rewrite the  $\phi$  integral as an  $l$  integral. To do so, write out an expression for  $l^2$ :

$$l^2 = (\vec{k} + \vec{q})^2 = k^2 + q^2 + 2\vec{k} \cdot \vec{q}, \quad (\text{B.8})$$

$$\vec{k} \cdot \vec{q} = kq (\cos \theta_{pq} \cos \theta_{pk} + \sin \theta_{pq} \sin \theta_{pk} \cos \phi) = \frac{l^2 - k^2 - q^2}{2} \quad (\text{B.9})$$

$$kq \cos \theta_{pq} \cos \theta_{pk} = \frac{(p^2 + q^2 - q'^2)(k'^2 - p^2 - k^2)}{4p^2} \quad (\text{B.10})$$

$$kq \sin \theta_{pq} \sin \theta_{pk} = \sqrt{(k^2 - k^2 \cos^2 \theta_{pk})(q^2 - q^2 \cos^2 \theta_{pq})} \quad (\text{B.11})$$

and hence

$$\cos \phi = \frac{p^4 + 2p^2 l^2 + k^2 q^2 + k'^2 q'^2 - (q^2 k'^2 + q'^2 k^2) - p^2 (k^2 + q^2 + k'^2 + q'^2)}{\sqrt{(2p^2 q^2 + 2p^2 q'^2 + 2q^2 q'^2 - p^4 - q^4 - q'^4)(2p^2 k^2 + 2p^2 k'^2 + 2k^2 k'^2 - p^4 - k^4 - k'^4)}}. \quad (\text{B.12})$$

Since the range of  $\cos \phi$  is from  $-1$  to  $+1$ , we find that the range of  $l^2$  at fixed  $p, k, q, k', q'$  is between

$$\frac{1}{2p^2} \left[ \left( p^2 (k^2 + q^2 + k'^2 + q'^2) + q^2 k'^2 + k^2 q'^2 - p^4 - k^2 q^2 - k'^2 q'^2 \right) \pm \sqrt{(2p^2 q^2 + 2p^2 q'^2 + 2q^2 q'^2 - p^4 - q^4 - q'^4)(2p^2 k^2 + 2p^2 k'^2 + 2k^2 k'^2 - p^4 - k^4 - k'^4)} \right], \quad (\text{B.13})$$

where the  $+$ ( $-$ ) sign represents the maximum (minimum) allowed value of  $l^2$ .

Differentiating the expression for  $\cos \phi$  holding  $p, k, q, k', q'$  fixed, we find

$$\sin \phi d\phi = \frac{4p^2 l dl}{\sqrt{(\dots)(\dots)}} \quad (\text{B.14})$$

where  $\sqrt{(\dots)(\dots)}$  is the same long square root in the above expressions. Therefore

$$d\phi = \frac{4p^2 l dl}{\sin \phi \sqrt{(\dots)(\dots)}}. \quad (\text{B.15})$$

Writing  $\sin \phi = \sqrt{1 - \cos^2 \phi}$  and after significant algebra we find

$$d\phi = \frac{2pl dl}{\sqrt{X}}, \quad (\text{B.16})$$

$$X = p^2 l^2 (k^2 + k'^2 + q^2 + q'^2 - p^2 - l^2) + q^2 k'^2 (k^2 + q'^2 + p^2 + l^2 - q^2 - k'^2) + k^2 q'^2 (q^2 + k'^2 + p^2 + l^2 - k^2 - q'^2) - k^2 k'^2 p^2 - q^2 q'^2 p^2 - k^2 q^2 l^2 - k'^2 q'^2 l^2. \quad (\text{B.17})$$

Note that the expression for  $X$  has a symmetry, if hard to see. The momenta are in three pairs;  $(p, l)$ ,  $(q, k')$ , and  $(q', k)$  which are ‘‘opposite’’ momenta in the diagram (momenta which do not touch at a vertex). The first terms involve pairs of ‘‘opposite’’ momenta, the last terms involve triples of momenta meeting at a vertex.

The total integration becomes

$$\frac{1}{2^4 \pi^7} \int \frac{p dp k dk q dq k' dk' q' dq' dl}{\sqrt{X}} \quad (\text{B.18})$$

with integration limits listed previously. We have not written the integration limits in a symmetric way, but they are symmetric.

The dot product of a pair of momenta which share a vertex are of form

$$\vec{p} \cdot \vec{k} = \frac{k'^2 - p^2 - k^2}{2}, \quad \vec{p} \cdot \vec{q} = \frac{p^2 + q^2 - q'^2}{2} \quad (\text{B.19})$$

where the sign difference is because in the first case the momenta are both directed out of the vertex while in the latter case one momentum enters and one exits the common vertex. For momenta which do not share a vertex, the dot product is

$$\vec{p} \cdot \vec{l} = \vec{p} \cdot (\vec{k} + \vec{q}) = \frac{q^2 + k'^2 - k^2 - q'^2}{2} \quad (\text{B.20})$$

and similarly for  $\vec{k} \cdot \vec{q}'$  and  $\vec{q} \cdot \vec{k}'$ . (For a mnemonic, note that  $q, k'$  are going from the beginning of one line to the end of the other;  $k, q'$  connect the beginnings of each line or the ends of each line.) We see that all dot products, including those for momenta on lines which do not meet at a vertex, have simple expressions in terms of momenta on lines.

As mentioned before, we can use the same integration variables for 3-loop diagrams with one or more 4-point vertices. For instance, when the  $l$  propagator is collapsed into a 4-point vertex, one can immediately do the  $l$  integral;

$$\int \frac{ldl}{\sqrt{X}} = \frac{\pi}{2p}. \quad (\text{B.21})$$

However, if the integrand involves dot products which depend on  $l$  then we cannot do the  $l$  integral immediately; we should instead interpret it as an angular integration which does not change the magnitudes of any momenta on the remaining lines, but which does affect some of their dot products.

## References

- [1] K. Kajantie, M. Laine, K. Rummukainen and M. Shaposhnikov, *Is there a hot electroweak phase transition at  $mH \geq mW$ ?*, *Phys. Rev. Lett.* **77** (1996) 2887.
- [2] F. Karsch, E. Laermann and A. Peikert, *Quark Mass and Flavour Dependence of the QCD Phase Transition*, *Nucl. Phys.* **B 605** (2001) 579 [hep-lat/0012023].
- [3] Y. Aoki, Z. Fodor, S.D. Katz and K.K. Szabo, *The QCD transition temperature: results with physical masses in the continuum limit*, *Phys. Lett.* **B 643** (2006) 46 [hep-lat/0609068].
- [4] P. de Forcrand and O. Philipsen, *The QCD phase diagram for small densities from imaginary chemical potential*, *Nucl. Phys.* **B 642** (2002) 290 [hep-lat/0205016].
- [5] A.G. Cohen, D.B. Kaplan and A.E. Nelson, *Progress in Electroweak Baryogenesis*, *Annu. Rev. Nucl. Part. Sci.* **43** (1993) 27.

- [6] J. M. Cline, *Baryogenesis*, arXiv:hep-ph/0609145.
- [7] M. Prakash, M. Prakash, R. Venugopalan and G. Welke, *Non-equilibrium properties of hadronic mixtures*, *Phys. Rep.* **227** (1993) 321.
- [8] A. Muronga and D. H. Rischke, *Evolution of Hot, Dissipative Quark Matter in Relativistic Nuclear Collisions*, arXiv:nucl-th/0407114.
- [9] A. Nakamura and S. Sakai, *Transport Coefficients of Gluon Plasma*, *Phys. Rev. Lett.* **94** (2005) 072305 [hep-lat/0406009].
- [10] H. Song and U. W. Heinz, *Extracting the QGP viscosity from RHIC data – a status report from viscous hydrodynamics*, *J. Phys.* **G 36** (2009) 064033 [arXiv:0812.4274].
- [11] R. Rapp and H. van Hees, *Heavy-Quark Diffusion, Flow and Recombination at RHIC*, *J. Phys.* **G 32** (2006) S351 [hep-ph/0606117];
- [12] R. Rapp and H. van Hees, *Heavy Quark Diffusion as a Probe of the Quark-Gluon Plasma*, arXiv:0803.0901.
- [13] B. Svetitsky, *Diffusion of charmed quarks in the quark-gluon plasma*, *Phys. Rev.* **D 37** (1988) 2484.
- [14] F. D. Steffen and M. H. Thoma, *Hard Thermal Photon Production in Relativistic Heavy Ion Collisions*, *Phys. Lett.* **B 510** (2001) 98 [hep-ph/0103044].
- [15] S. Turbide, R. Rapp and C. Gale, *Hadronic Production of Thermal Photons*, *Phys. Rev.* **C 69** (2004) 014903 [hep-ph/0308085].
- [16] PHENIX COLLABORATION, G. David, *Direct Photons at RHIC*, arXiv:0810.0872.
- [17] K. Kajantie, M. Laine, K. Rummukainen and Y. Schröder, *The pressure of hot QCD up to  $g^6 \ln(1/g)$* , *Phys. Rev.* **D 67** (2003) 105008 [hep-ph/0211321].
- [18] E. Braaten and R.D. Pisarski, *Soft amplitudes in hot gauge theories: A general analysis*, *Nucl. Phys.* **B 337** (1990) 569.
- [19] P. Arnold, G. D. Moore and L. G. Yaffe, *Effective Kinetic Theory for High Temperature Gauge Theories*, *JHEP* **0301** (2003) 030 [hep-ph/0209353].
- [20] P. Arnold, G. D. Moore and L. G. Yaffe, *Transport coefficients in high temperature gauge theories: (II) Beyond leading log*, *JHEP* **0305** (2003) 051 [hep-ph/0302165].
- [21] S. Caron-Huot and G. D. Moore, *Heavy quark diffusion in QCD and  $\mathcal{N} = 4$  SYM at next-to-leading order*, *JHEP* **0802** (2008) 081 [arXiv:0801.2173].
- [22] S. Caron-Huot,  *$O(g)$  plasma effects in jet quenching*, *Phys. Rev.* **D 79** (2009) 065039 [arXiv:0811.1603].
- [23] J. M. Cornwall, R. Jackiw and E. Tomboulis, *Effective action for composite operators*, *Phys. Rev.* **D 10** (1974) 2428.
- [24] J. Berges,  *$n$ -Particle irreducible effective action techniques for gauge theories*, *Phys. Rev.* **D 70** (2004) 105010 [hep-ph/0401172].
- [25] T. Appelquist and R. D. Pisarski, *High-temperature Yang-Mills theories and three-dimensional quantum chromodynamics*, *Phys. Rev.* **D 23** (1981) 2305.
- [26] E. Braaten and A. Nieto, *Effective field theory approach to high-temperature thermodynamics*, *Phys. Rev.* **D 51** (1995) 6990 [hep-ph/9501375].

- [27] K. Kajantie, M. Laine, K. Rummukainen and M. Shaposhnikov, *3d  $SU(N)$  + adjoint Higgs theory and finite-temperature QCD*, *Nucl. Phys.* **B 503** (1997) 357 [hep-ph/9704416].
- [28] J. S. Ball and T. W. Chiu, *Analytic properties of the vertex function in gauge theories. I*, *Phys. Rev.* **D 22** (1980) 2542.
- [29] A. I. Davydychev, P. Osland and O. V. Tarasov, *Three-gluon vertex in arbitrary gauge and dimension*, *Phys. Rev.* **D 54** (1996) 4087 [hep-ph/9605348].
- [30] A. K. Rajantie, *Feynman diagrams to three loops in three-dimensional field theory*, *Nucl. Phys.* **B 480** (1996) 729 [Erratum *ibid* **B 513** (1998) 761] [hep-ph/9606216].
- [31] R. Alkofer and L. von Smekal, *The infrared behavior of QCD Green's functions – Confinement, dynamical symmetry breaking, and hadrons as relativistic bound states*, *Phys. Rept.* **353** (2001) 281 [hep-ph/0007355].
- [32] V. N. Gribov, *Quantization of non-Abelian gauge theories*, *Nucl. Phys.* **B 139** (1978) 1.
- [33] D. Zwanziger, *Vanishing of zero-momentum lattice gluon propagator and color confinement*, *Nucl. Phys.* **B 364** (1991) 127.
- [34] L. von Smekal, A. Hauck and R. Alkofer, *A solution to coupled Dyson-Schwinger equations for gluons and ghosts in Landau gauge*, *Annals Phys.* **267** (1998) 1 [Erratum *ibid* **269** (1998) 182] [hep-ph/9707327].
- [35] D. Zwanziger, *Non-perturbative Landau gauge and infrared critical exponents in QCD*, *Phys. Rev.* **D 65** (2002) 094039 [hep-th/0109224].
- [36] P. Boucaud et. al., *The Infrared Behavior of the Pure Yang-Mills Green Functions*, arXiv:hep-ph/0507104.
- [37] A. C. Aguilar, D. Binosi and J. Papavassiliou, *Gluon and ghost propagators in the Landau gauge: Deriving lattice results from Schwinger-Dyson equations*, *Phys. Rev.* **D 78** (2008) 025010 [arXiv:0802.1870].
- [38] C. S. Fischer, A. Maas and J. M. Pawłowski, *On the infrared behavior of Landau gauge Yang-Mills theory*, *Annals Phys.* **324** (2009) 2408 [arXiv:0810.1987].
- [39] I. L. Bogolubsky, E.-M. Ilgenfritz, M. Müller-Preussker and A. Sternbeck, *The Landau gauge gluon and ghost propagators in 4D  $SU(3)$  gluodynamics in large lattice volumes*, *PoS(LATTICE 2007)* (2007) 290 [arXiv:0710.1968].
- [40] I.L. Bogolubsky, E.-M. Ilgenfritz, M. Müller-Preussker and A. Sternbeck, *Lattice gluodynamics computation of Landau-gauge Green's functions in the deep infrared*, *Phys. Lett.* **B 676** (2009) 69 [arXiv:0901.0736].
- [41] O. Oliveira and P. J. Silva, *The lattice infrared Landau gauge gluon propagator: from finite volume to the infinite volume*, *PoS(QCD-TNT 09)* (2009) 033 [arXiv:0911.1643].
- [42] A. Cucchieri and T. Mendes, *What's up with IR gluon and ghost propagators in Landau gauge? A puzzling answer from huge lattices*, *PoS(LATTICE 2007)* (2007) 297 [arXiv:0710.0412].
- [43] A. Cucchieri and T. Mendes, *Constraints on the IR behavior of the ghost propagator in Yang-Mills theories*, *Phys. Rev.* **D 78** (2008) 094503 [arXiv:0804.2371].
- [44] A. Cucchieri, D. Dudal, T. Mendes and N. Vandersickel, *Modeling the gluon propagator in Landau gauge: lattice estimates of pole masses and dimension-two condensates*, arXiv:1111.2327.

- [45] A. Cucchieri, T. Mendes and E. M. da S. Santos, *Simulating linear covariant gauges on the lattice: a new approach*, *PoS(QCD-TNT 09)* (2009) 009 [arXiv:1001.2002].
- [46] P. Cvitanovic, P. G. Lauwers and P. N. Scharbach, *Gauge invariance structure of quantum chromodynamics*, *Nucl. Phys. B* **186** (1981) 165.
- [47] M. Laine and O. Philipsen, *The Nonperturbative QCD Debye mass from a Wilson line operator*, *Phys. Lett. B* **459** (1999) 259 [hep-lat/9905004].
- [48] P. Arnold and L. G. Yaffe, *The NonAbelian Debye screening length beyond leading order*, *Phys. Rev. D* **52** (1995) 7208 [hep-ph/9508280].
- [49] A. Hietanen, K. Kajantie, M. Laine, K. Rummukainen and Y. Schröder, *Plaquette expectation value and gluon condensate in three dimensions*, *JHEP* **0501** (2005) 013 [hep-lat/0412008].
- [50] E. E. Boos and A. I. Davydychev, *A method of calculating massive Feynman integrals*, *Theor. Math. Phys.* **89** (1991) 1052.